Marine and Petroleum Geology 141 (2022) 105690

Contents lists available at ScienceDirect

Marine and Petroleum Geology

journal homepage: www.elsevier.com/locate/marpetgeo

Seismic characterization and modelling of the gas hydrate system in the northern Bay of Bengal, offshore Bangladesh

Vanessa Monteleone [a,b,*], Héctor Marín-Moreno [b,c], Gaye Bayrakci [b], Angus Best [b], Farhana Shaon [d], Mohammad Moinul Hossain [e], Ahmad Al Karim [f], Md Khurshed Alam [f]

[a] School of Ocean and Earth Science, University of Southampton, National Oceanography Centre Southampton, Waterfront Campus, European Way, Southampton, SO14 3ZH, UK
[b] National Oceanography Centre, European Way, Southampton, SO14 3ZH, UK
[c] Norwegian Geotechnical Institute, PB 3930 Ullevål Stadion, NO-08906, Oslo, Norway
[d] Bangladesh Oil, Gas and Mineral Corporation (Petrobangla), Dhaka, Bangladesh
[e] Bangladesh Petroleum Exploration and Production Company Limited (BAPEX), Dhaka, Bangladesh
[f] Maritime Affairs Unit, Ministry of Foreign Affairs, Dhaka, 1000, Bangladesh

ARTICLE INFO

Keywords:
Gas hydrate
Bangladesh
Seismic reflection data
BSR
Gas migration
Geothermal gradient
Gas hydrate stability modelling

ABSTRACT

The offshore Bangladesh includes the northern Bengal fan, where sediment supply from the Ganges and Brahmaputra rivers has resulted in the accumulation of up to 20 km of shallow-marine, fluvio-deltaic and slope sediments that have accumulated during rapid tectonic subsidence since the late Miocene. The high sedimentation rates, along with high organic matter content, make this area favorable for the formation of natural gas from both microbial and thermogenic sources. Here we use multichannel seismic reflection profiles and modelling of the gas hydrate stability zone (GHSZ) to present the first evidence for the occurrence of natural gas hydrate in the offshore Bangladesh. First, we analyze the sediments of the shelf and slope areas, which are characterized by downslope sediment transport features and by the presence, in places, of faults/fractures as well as widely distributed amplitude anomalies and seismic facies that we relate to the presence of gas. A high-amplitude reversed polarity reflection of variable continuity that mimics the seafloor and cross-cut stratigraphy is interpreted as a Bottom Simulating Reflector (BSR). The BSR is observed in several areas that are predominantly located in the E-SE of the study area, in water depths of 1300–1900 m and at depths below seafloor of 250–440 m. Sediments above BSR locations generally show higher seismic interval velocities reaching values of ~1920–1940 m/s, which are consistent with the presence of gas hydrate in shallow marine sediments. Furthermore, the BSR lies at approximately the same depth as the theoretical base of the gas (methane) hydrate stability zone (BGHSZ), calculated assuming a 3.5 % wt pore water salinity and using existing geothermal gradient and seafloor temperature data from the study region. However, in places, the BSR lies deeper or shallower than the base of the modelled BGHSZ. These discrepancies include areas where faults/fractures and seismic evidence linked to fluid flow from deeper reservoirs reach the GHSZ disrupting its stratigraphic continuity. At these locations, we suggest that faults/fractures act as fluid migration pathways causing localized heat-flow perturbations and/or changes in the hydrate-forming gas composition both likely affecting the depth of the GHSZ. Our results provide the first evidence of the gas hydrate potential in the offshore Bangladesh and should drive future research and data acquisition aiming to understand the composition, saturation and thickness of the gas hydrate-bearing sediments in this region.

1. Introduction

Gas hydrate is an ice-like crystalline solid, comprising a hydrogen-bonded water lattice with trapped gas molecules, that is stable at high pressures and low temperatures (e.g., Sloan and Koh, 2008). It is found in nature in marine settings, including continental margins and deep marine sediments, as well as in sub-glacial and permafrost environments (e.g., Ruppel, 2015; Portnov et al., 2016; Boswell et al., 2020).

* Corresponding author. Wood Thilsted Partners Ltd., 1st Floor, 91 – 94 Lower Marsh, London, SE1 7AB, UK.
E-mail address: vanessamonteleone88@gmail.com (V. Monteleone).

https://doi.org/10.1016/j.marpetgeo.2022.105690
Received 12 September 2021; Received in revised form 10 April 2022; Accepted 11 April 2022
Available online 15 April 2022

Submarine gas hydrate formation depends on factors such as the availability, composition and source of gas, pore-size distribution, pore-water salinity, geothermal gradient and seafloor temperature (Dickens and Quinby-Hunt, 1997; Kvenvolden and Lorenson, 2001; Moridis and Collett, 2003). The most abundant hydrate-forming gas in marine sediments is methane (CH_4), commonly with small amounts of hydrogen sulfide (H_2S), carbon dioxide (CO_2), and other small molecule gases, due to the bacterial breakdown of organic matter within the shallow sediments (e.g., Kvenvolden, 1993; Sloan, 1998, 2003; Stern et al., 2011). The presence of heavier hydrocarbons (i.e., ethane, propane) is less common, and is associated with thermo-catalytic production at depth via heating of buried kerogen (e.g., Sloan, 2003; Lu et al., 2007; Bourry et al., 2009). Gas hydrate has the potential to be an important future energy resource, especially in countries that lack other indigenous fossil fuel resources (e.g., Kvenvolden, 1993; Grauls, 2001; Collett et al., 2009; Boswell and Collett, 2011; Arora et al., 2015; Boswell et al., 2020). Vast research programs have been undertaken by countries including the United States, Canada, Japan, India, South Korea, and China in order to explore the long-term goal of exploiting gas hydrates as energy resource in a cost effective and safe manner (e.g., Collett et al., 2014; Arora et al., 2015; Han et al., 2019).

Multidisciplinary investigations using geophysical techniques (e.g., seismic reflection and refraction, electromagnetic surveys, well logging) as well as geochemical analyses have been extensively used to explore gas hydrate accumulations on continental margins and permafrost regions (e.g., Minshull et al., 2020). Scientific ocean drilling has provided log and core data to assess the characteristics of gas hydrate deposits, and to test methods for their exploration and production (e.g., Collett et al., 2014, 2019; Boswell et al., 2020). Seismic reflection data may be used to identify the base of the gas hydrate stability zone (BGHSZ) beneath the seafloor, which manifests as a high amplitude seismic reflection with negative impedance contrast known as a Bottom Simulating Reflector (BSR) (Shipley et al., 1979; Brown et al., 1996; Andreassen et al., 1997). BSRs can arise at the boundary between a gas hydrate-bearing layer with high-velocity overlying sediments with a normal velocity (Hyndman and Davis, 1992; Hyndman and Spence, 1992), though they more commonly identify the boundary between sediments containing gas hydrate underlain by a low-velocity zone, typically a few meters to many tens of meters thick, in which there is a small proportion of free gas within the pore space (e.g., Miller et al., 1991; Singh et al., 1993; MacKay et al., 1994; Hovland et al., 1997). Note that the lack of a BSR in an area where stability conditions are present does not necessary imply the absence of gas hydrate (e.g., Chabert et al., 2011; Riedel et al., 2011). Seismic evidence of gas accumulations and migration pathways within the GHSZ, such as gas chimneys and pipes, can also be considered as indirect indicators for the presence of gas hydrate (e.g., Judd and Hovland, 1992) as they show the potential availability of gas for hydrate formation.

In this study, we investigate the likely occurrence of natural gas hydrate deposits in the northern Bay of Bengal (BoB), within the Bangladesh Exclusive Economic Zone (EEZ) (Fig. 1). Bangladesh is one of the world's most densely populated countries and relies on natural gas for much of its energy needs (Masud et al., 2020). However, as domestic reserves are rapidly depleting, the country is now exploring the possibility of developing renewable energy resources and unconventional fossil fuels to sustain the continuous increase in its energy demand (Masud et al., 2020). West of Bangladesh, along the eastern Indian continental margin (Fig. 1), results from expeditions of the Indian National Gas Hydrate Program (NGHP) have proven the presence of conspicuous amounts of gas hydrate accumulations in the Krishna-Godavari and Mahanadi Basins (e.g., Collett et al., 2008, 2014; Ramana et al., 2009; Riedel et al., 2011; Lorenson and Collett, 2018; Shukla et al., 2019) (Fig. 1). To the east of Bangladesh, large gas fields (Shwe, Shwe phu, Mia; Fig. 1) associated with Pliocene turbidites have also been

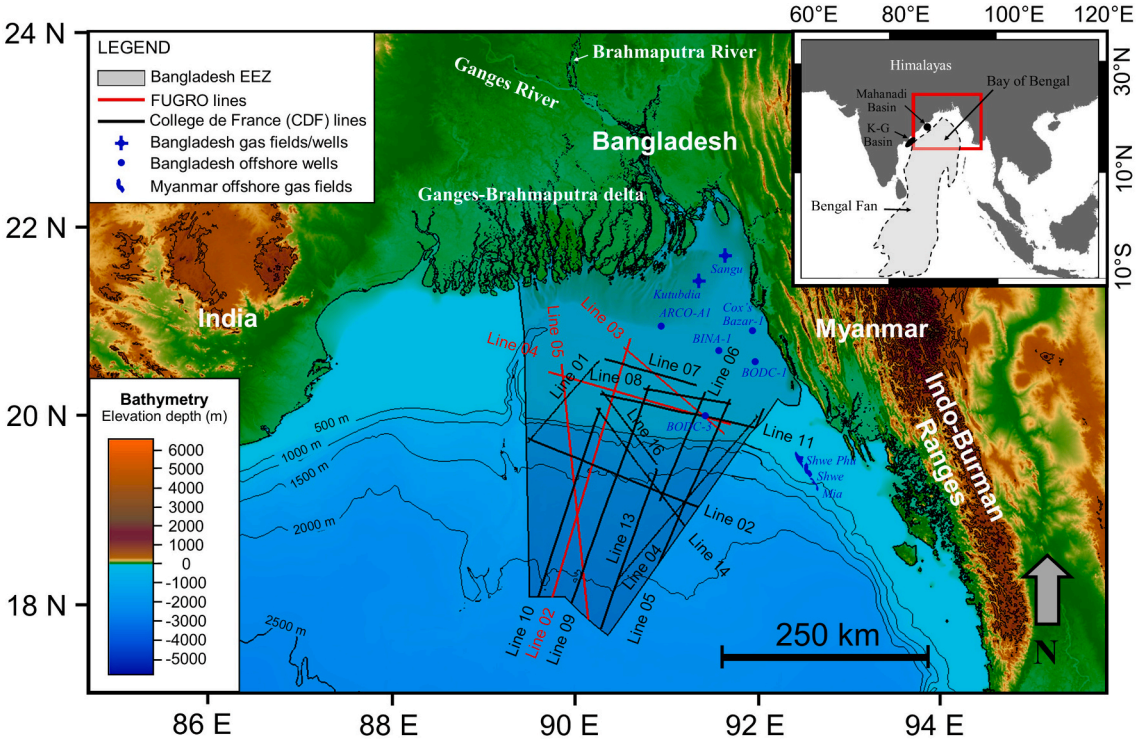

Fig. 1. Bathymetric map of the northern Bay of Bengal (BoB) (https://www.gebco.net/) bounded by the east India continental margin to the west, Bangladesh in the north, and the Indo-Burman Ranges (Myanmar) to the east. Within the Bangladesh Exclusive Economic Zone (EEZ), lines and symbols show the locations of seismic reflection profiles used in this study and of wells used for geothermal gradient estimates (Guha et al., 2010; Akbar, 2011). Also shown are the locations of gas fields offshore Bangladesh (Curiale et al., 2002) and Myanmar (Yang and Kim, 2014). At top right, inset map shows the extent of the Bengal Fan, and the location of the Mahanadi and Krishna-Godavari (K–G) Basins offshore east India (e.g., Shukla et al., 2019).

discovered in the offshore Myanmar in close proximity to Bangladesh shallow offshore exploration blocks (e.g., Yang and Kim, 2014; Zhan et al., 2019; Ma et al., 2020). Within the Bangladesh EEZ, the Sangu and Kutubdia gas fields and other non-commercial hydrocarbon fields (Fig. 1), and the high amounts of methane and other higher molecular weight hydrocarbon gases detected in the water column and in the thick sedimentary infill, indicate the existence of both deep and shallow gas reservoirs (e.g., Curiale et al., 2002; Berner et al., 2003). The proximity and similarity to the tectono-stratigraphy of gas hydrate prospective areas offshore eastern India, and the evidence for hydrocarbon systems both offshore Myanmar and within the Bangladesh EEZ itself, are good indicators for the presence of gas hydrates within the Bangladesh EEZ. However, to our knowledge, no published studies have yet investigated the occurrence of natural gas hydrate in this area.

In this study, we present a first assessment of the presence and distribution of gas hydrates within the Bangladesh EEZ, using 2D multichannel seismic reflection data. The study is sponsored by the Government of Bangladesh and the data is obtained from the Ministry of Foreign Affairs (MOFA), Petrobangla and its subsidiary Bangladesh Petroleum Exploration and Production company (BAPEX). Based on the data provided, we first describe the sedimentary successions of the Bangladesh continental shelf and slope areas, and present evidence for gas indicators, including a discontinuous BSR. We identify seismic interval velocities indicative of gas/gas hydrate-bearing sediments and use them to provide a qualitative estimate for gas hydrate saturation of sediments. We then model the theoretical base of the methane gas hydrate stability zone and compare it to the observed depth of the BSR. Discrepancies between observations and model results are discussed in terms of possible controls on the gas hydrate system. Our findings provide insights on the gas hydrate potential of this frontier area and can help to guide the planning of future exploration and drilling programs offshore Bangladesh.

2. Regional geologic setting

The Bay of Bengal (BoB) represents the north-eastern extension of the Indian Ocean, bordered by India, Bangladesh and the Indo-Burman Ranges of Myanmar (Fig. 1), and contains a sedimentary depocenter comprised of up to 20 km of Oligocene to Recent sediments (Curray and Munasinghe, 1989; Curiale et al., 2002; Alam et al., 2003). Basin evolution started in early Cretaceous time with the rifting of the Indian Plate away from Antarctica (e.g., Coffin and Lawver, 1998; Curray, 2014). However, the basin did not become a major depocenter until late Eocene time, when the northward-drifting Indian Plate collided with the Eurasia Plate resulting in the initial uplift of the Himalayan and Indo-Burman Ranges (Curray et al., 1982; Lindsay et al., 1991). During Oligocene to late Miocene time, the basin began to fill with sediments derived from the rising Himalayas and transported basinward by large river systems (Curray et al., 2003). During late Miocene and Holocene time, a major phase of continental collision ("hard" collision) caused the rapid uplift of the Himalayas and consequent subsidence of the basin to the south (Curray et al., 2003). Increasing amounts of erosional detritus derived from the Himalayas were transported mainly by the Ganges-Brahmaputra River system to the offshore area during this time, forming a prograding delta system and distributing sediments downslope and into the deep ocean via turbidity currents (Curray et al., 2003). Late Tertiary sediments of the BoB are therefore represented by fluvio-deltaic to shallow-marine and deep-marine turbidite deposits, overlain by southward prograding deltaic sequences (Curray and Moore, 1971). This delta system has advanced over time to form the world's largest submarine fan complex, the Bengal Fan, extending over the entire BoB from 20°N at 1400 m water depth to 7°S at 5000 m water depth over a N–S length of 3000 km (Curray and Moore, 1971).

The Bangladesh EEZ extends seaward to water depths of 2250 m and comprises the upper part of the Bengal Fan (Fig. 1). Here, up to 20 km of mostly Tertiary siliciclastic sediments, including deep-to shallow-marine, deltaic and fluvial facies were deposited at high sedimentation rates and contain large amounts of terrestrially sourced organic carbon (e.g., Brune et al., 1992; Curray, 1994; Ramana et al., 2009). The rapid burial of organic-rich sediments favors microbial methane generation (e.g., Ramana et al., 2009), while the presence of multiple deep petroleum systems indicates likely deeper sources supplying thermogenic gas (Curiale et al., 2002). Together with generally low geothermal gradients in this region (25–30 °C/km; e.g., Guha et al., 2010; Akbar, 2011) favoring the development of a thick GHSZ (Sloan and Koh, 2008), these factors make the offshore Bangladesh EEZ a promising location for the occurrence of natural gas hydrate.

3. Data and methods

3.1. Seismic data

This study is based on 2D multichannel seismic reflection profiles acquired during two surveys. Thirteen pre-stack time migrated seismic profiles belong to a College de France (CDF) and TOTAL survey acquired in 2007–2008 (Fig. 1). The profiles were acquired using a 10.5 km-long streamer with 804 channels towed at water depth of 8 m, and a 6180 in^3 tuned air-gun array of 64 air-guns towed at a water depth of 8 m and a 50 m shooting interval. Four other post-stack time migrated seismic reflection profiles were acquired by Fugro Geoteam AS in 2010 (Fig. 1). This survey used a 12 km-long streamer with 960 channels towed at a water depth of 11 m, and a 6300 in^3 single air-gun source towed at a water depth of 10 m and a 50 m shooting interval. For both surveys, the processing sequence included SEGY reformatting, navigation merging, amplitude correction, de-signature and zero-phasing, band-pass filtering, noise attenuation, trace editing, velocity analysis, de-multiple (Radon and 2D SRME), and Kirchhoff pre-stack (for CDF/TOTAL profiles) and post-stack (for FUGRO profiles) time migration. CDF/TOTAL and FUGRO data are characterized by a dominant frequency of ~35 Hz and ~25 Hz within few hundred meters below seafloor, respectively. Thus, the expected vertical resolution for each dataset is ~12 m and ~17 m within the top few hundred meters depth below seafloor, assuming sediment seismic velocity of 1700 m/s.

Manually picked root-mean-squared (RMS) and interval stacking velocities are available at a 500 m interval along the Fugro profiles and at a 5 km interval along the CDF profiles, which we used to convert the seismic profiles into depth. Velocities show a vertical picking interval of ~100 ms, thus providing a coarse vertical resolution.

The seismic reflection profiles were used to identify variations in seismic facies indicative of key sedimentary features (i.e., mass transport deposits, channel complexes and hemipelagic deposits) along the Bangladesh continental shelf and slope areas. Furthermore, the presence of anomalous seismic amplitude reflections was used to define the presence of potential BSRs and other indirect (i.e., bright spots, gas chimneys) evidence for gas hydrate accumulations (Figs. 2–5). Interval stacking velocities were also used to investigate the presence of anomalous high- and low-velocity zones within the shallow sediments, which could be related to gas hydrate-bearing and gas-bearing zones, respectively (e.g., Lee, 2004; Chabert et al., 2011; Riedel et al., 2014) (Fig. 5).

Various seismic attributes were used to examine the frequency and amplitude characteristics of gas-charged sediments (Fig. 4). A root-mean-square (RMS) seismic attribute, which calculates the square root of the sum of the squared amplitudes divided by the number of samples within the specified window (e.g., Chen and Sidney, 1997), was used to enhance seismic amplitude anomalies related to gas and/or gas hydrate accumulations along seismic profiles (Fig. 4B). Similar results are given by the Envelope seismic attribute, also known as "Instantaneous amplitude" or "Reflection strength", which calculates the instantaneous magnitude of the analytic signal independent of phase (e.g., Taner et al., 1979; Chen and Sidney, 1997) (Fig. 4C). Finally, a Coherency seismic attribute was calculated to illuminate faults and discontinuities and to identify chaotic textures associated with gas migration pathways,

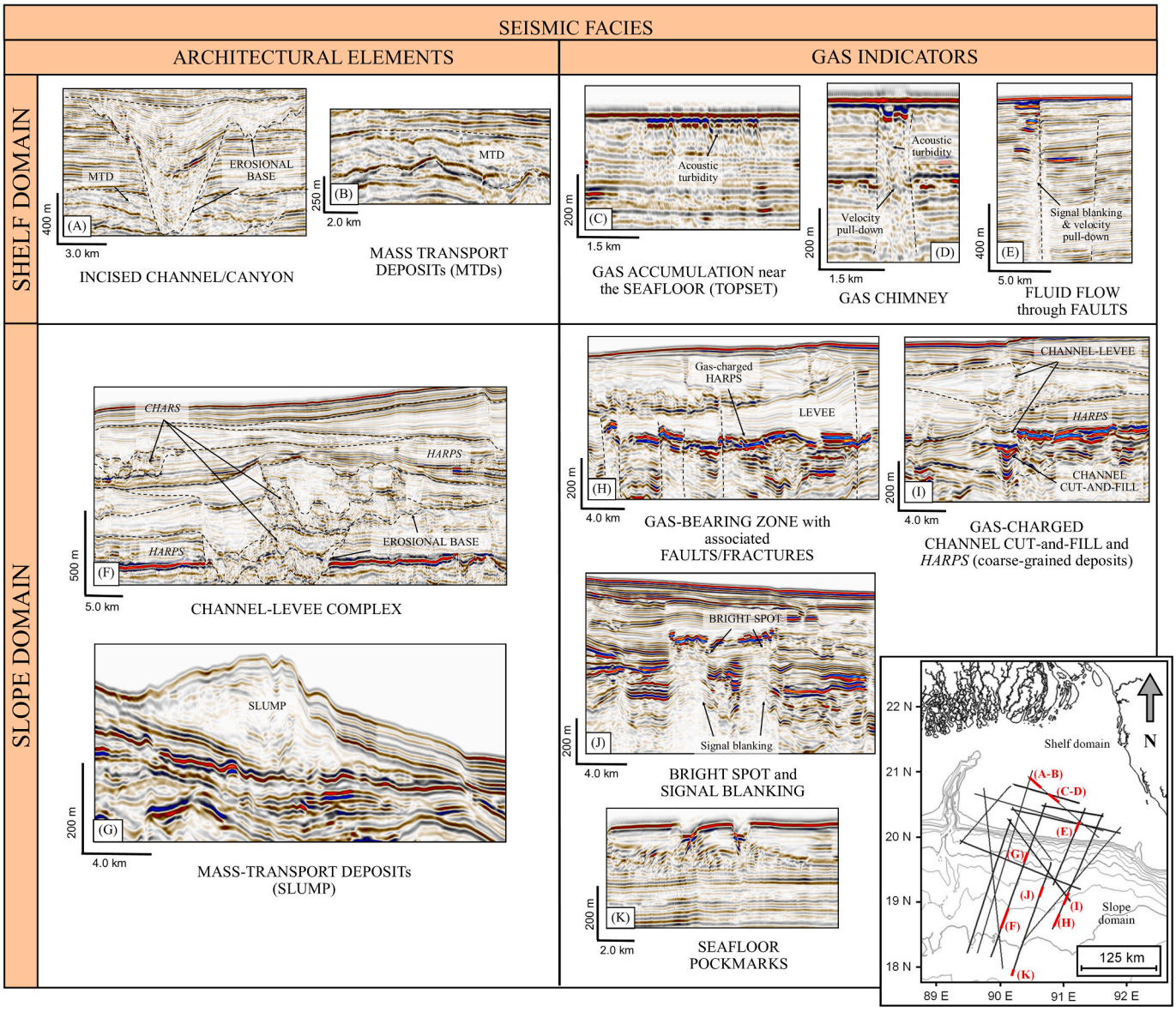

Fig. 2. Seismic profiles illustrating sedimentary architectural elements and seismic facies, and anomalies indicative of gas along the Bangladesh continental shelf (A-E) and slope (F–K) domains (locations are shown in the inset map). On the shelf, architectural elements consist of (A) incised channels/canyons and (A-B) mass-transport-deposits (MTDs). Gas indicators are visible as high amplitude anomalies (bright spots) showing (C) gas-charged layers or (D) gas pockets. Signal blanking and velocity pull-down effects are related to focused gas migration pathways such as (D) gas chimneys and (E) faults. In the slope domain, architectural elements are (F) channel-levee complexes, filled by chaotic high-amplitude reflectors (CHARS) and intercalated with high amplitude reflection packages (HARPS) associated with channel avulsion and turbidite overflow, and (G) MTDs (i.e., slumps) recording slope failure. Gas indicators are (H–I) bright spots associated with channel cut-and-fill and turbidite overflow deposits, (H) faults/fractures terminating at/close to the high amplitude anomalies and probably acting as fluid pathways, (J) signal blanking effects beneath some bright spots, and (H) seafloor pockmarks indicating fluid migration and escape through the seafloor.

chaotic channel infill, etc. (Fig. 4D). This attribute, which is scaled from 0 to 1, estimates the chaotic signal pattern contained within seismic data measured as the lack of organization in the dip and azimuth estimation method (e.g., Marfurt et al., 1999). To ensure good results, seismic attributes were calculated using short window lengths defined by a number of samples equal to 9 and 33, and by a directional window radius of 1.5 by 1.5, for the respective attributes.

3.2. Gas hydrate saturation estimate

Interval velocities available from seismic data (P-wave velocities) were used to estimate the amount of gas hydrate in sediments using rock physics models linking seismic velocity to the internal rock structure (e.g., Chand et al., 2004; Westbrook et al., 2008). The Hydrate-Bearing Effective Sediment (HBES) model described by Marín-Moreno et al. (2017) was used to calculate the P-wave velocity based on a sediment composed by mineral grains and variable amounts of brine, gas, and gas hydrate in the pore space. The Marín-Moreno et al. (2017) model builds on the approach of Ecker et al. (1998), who considered two idealized models for gas hydrate formation in the pore space of sand uncemented (for pore floating hydrate) and cemented (for cemented hydrate) sand models (Dvorkin and Nur, 1996; Mavko et al., 2009). These models are used to calculate the frame properties of the dry rock and introduced into the Biot-Stoll model (Biot, 1596a, 1596b; Stoll and Bryan, 1970) to obtain the elastic properties of the gas hydrate bearing sediment.

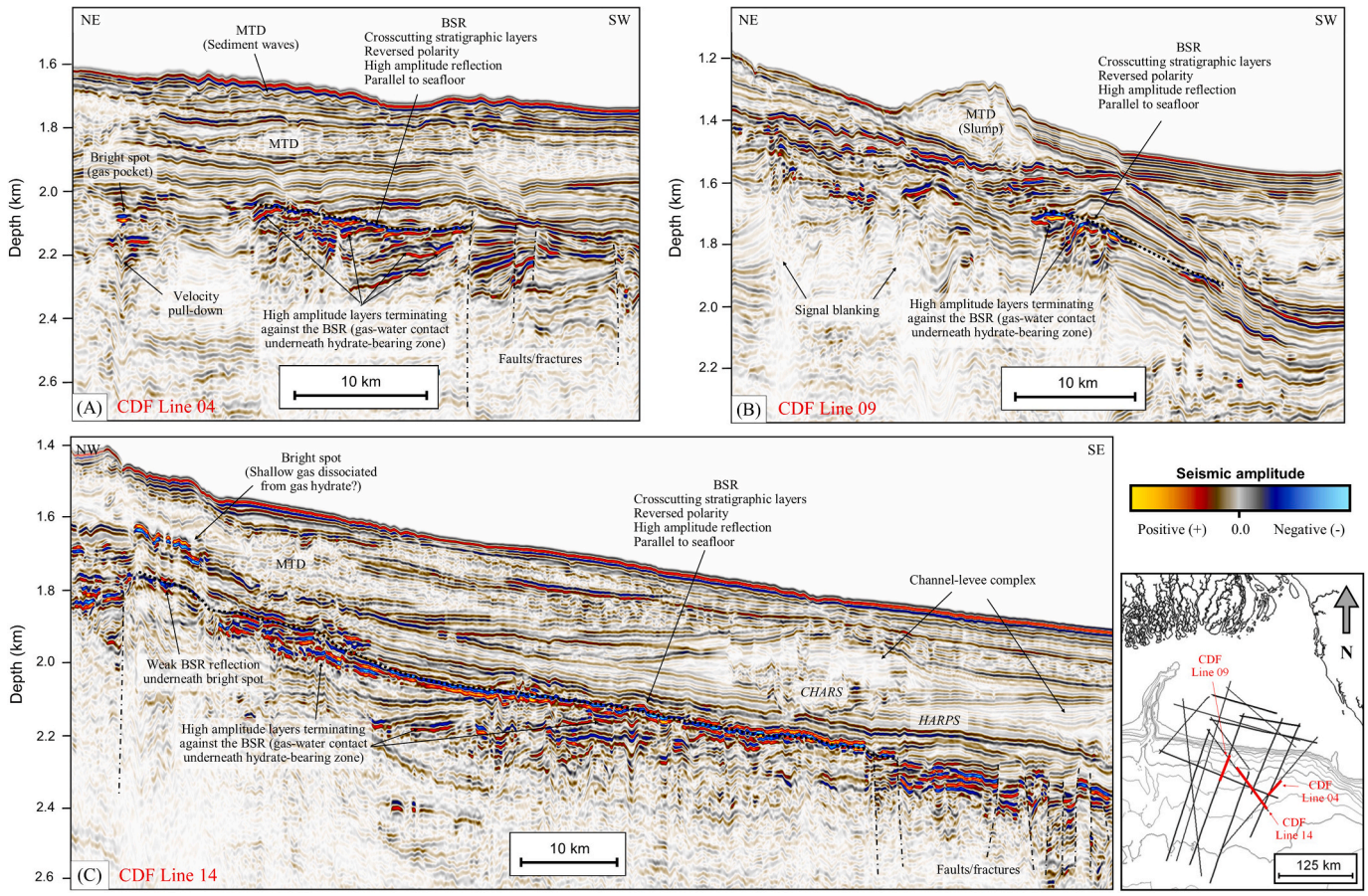

Fig. 3. Seismic reflection profiles across the slope domain: (A) CDF Line 04, (B) CDF Line 09, (C) CDF Line 14 (location shown in inset map). In (A) and (B), BSRs (dotted black lines) are visible as continuous to discontinuous, high amplitude, reversed polarity reflections that parallel the seafloor and crosscut stratigraphy. High amplitude layers are visible beneath the BSR, interpreted as gas-water contacts underneath the gas hydrate-bearing region. MTDs (slumps and wavy sediments) are visible, indicating events of slope failure. In (C), the BSR appears as a more continuous reflection crosscutting stratigraphy. In the NW, the BSR is partly obscured by blanking due to a suprajacent bright spot, which may indicate that gas has migrated through the GHSZ following hydrate destabilization and dissociation. In the SE, faults/fractures disrupt the continuity of the BSR.

3.3. Modelling of the BGHSZ

Modelling of the thickness of the gas hydrate stability zone (GHSZ) below the seafloor is used to complement and guide seismic interpretation, as this provides the sub-seafloor depth for the base of the gas hydrate stability zone (BGHSZ) which can be compared against the depth of the BSR. The GHSZ thickness is given by the distance between the seafloor and the intersection of the temperature profile with a gas hydrate phase boundary (Marín-Moreno et al., 2016). Hence, assuming hydrostatic pore fluid pressure, this calculation depends upon parameters such as bathymetry, geothermal gradient, seafloor temperature, pore-water salinity, and molecular composition of the hydrate-forming gas (e.g., MacLeod, 1982; Sloan, 1998).

We compiled bathymetry, temperature, salinity, and geothermal gradient data from the literature and available databases to define the model parameters. We relied on published literature for values of geothermal gradient in the Bangladesh offshore area, which were calculated from corrected bottom-hole temperatures at abandoned exploration well locations (Ismail and Shamsuddin, 1991; Guha et al., 2010; Akbar, 2011) (Fig. 1). Seafloor temperatures were available from the NOAA database at 100 m water depth-intervals within our study area (https://www.nodc.noaa.gov/OC5/woa18f/; Locarnini et al., 2019). We calculated average temperature values for each 100 m interval and linearly interpolated them to create a smooth profile of decreasing temperature with increasing water depth (Figure S1). Note that we assume that seafloor temperature changes are only dependent on water depth.

Our models consider 100% methane hydrate (Moridis, 2003), 3.5% wt pore water salinity (Miles, 1995), seafloor temperatures between 5.3 °C and 2.7 °C (https://www.nodc.noaa.gov/OC5/woa18f/; Locarnini et al., 2019) corresponding to the water depths where BSRs are identified (1300–1900 m bMSL) (Figure S1), and geothermal gradients estimated from offshore wells between 25 °C/km and 30 °C/km (well locations in Fig. 1; Guha et al., 2010; Akbar, 2011). We used a range of seafloor temperatures and geothermal gradients to consider their uncertainty and impact on the calculated depth of the BGHSZ. The Dickens and Quinby-Hunt (1997) relationship was used to consider pore water salinity effects in Moridis (2003) freshwater methane hydrate stability curve. We assumed hydrostatic conditions and converted depth to pressure with a water density of 1030 kg m^{-3}.

The calculated BGHSZ and the observed BSR may differ if the seismic velocities used for time-depth conversion of the seismic data are inaccurate. Also, differences may occur if the observed BSR represents a gas hydrate system affected by heat-flows anomalies, and/or variable hydrate-forming gas composition (e.g., Ruppel and Kessler, 2017). We do not have constraints on spatial variations in the temperature field, nor on the composition of the hydrate-forming gas, but we accounted for possible time-depth conversion related errors by calculating BSR depth error range for an interval velocity variation between - 100 m/s and +200 m/s. Such stacking velocities variation was considered reasonable within our depth of interest, which extends to approximately 500 m below seafloor (mbsf). Over this depth range, the maximum decrease of -

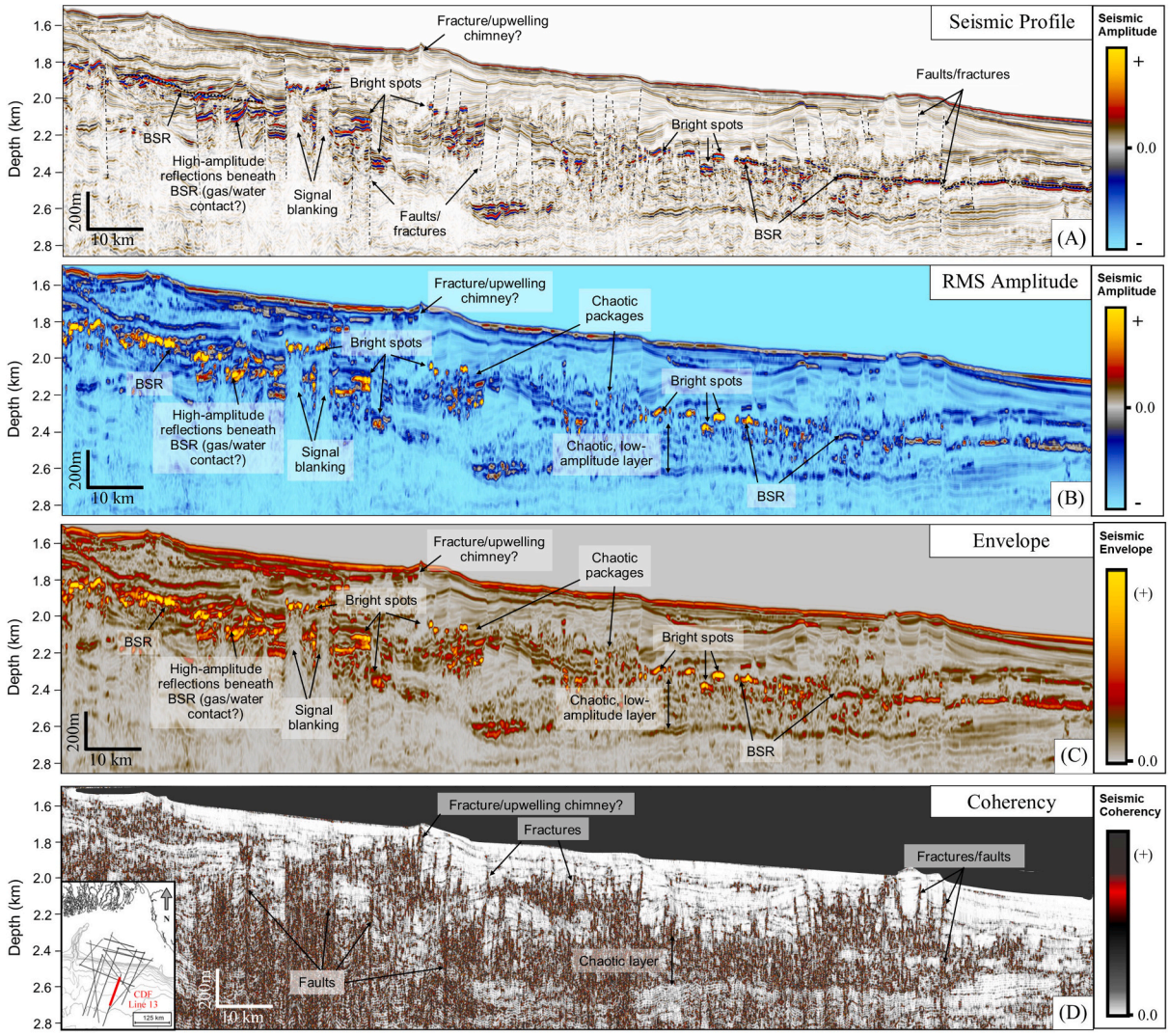

Fig. 4. Seismic attributes along CDF Line13. (A) Original seismic profile with some interpretation in overlay. The BSR is discontinuous along this profile, disrupted by bright spots, faults/fractures, and signal blanking effects. High amplitude reflections are visible beneath the BSR at the left side of the profile, interpreted as gas-charged sediments (top) and gas-water contacts (bottom). (B) RMS Amplitude and (C) Envelope seismic attributes which enhance bright spots and BSR related reflections, as well as signal blanking effects associated with gas accumulations and migration pathways. A chaotic, low-amplitude layer is visible beneath the discontinuous BSR on the central to right of the profile. (D) Coherency seismic attribute, which enhances the presence of chaotic sequences linked to gas- and/or gas hydrate-bearing zones, and lateral discontinuities related to the presence of faults/fractures.

100 m/s was set to prevent sediment velocities from becoming too close, or lower than, water velocity. A larger maximum velocity increase of +200 m/s was set in order to not exceed the average maximum velocity expected for sediments within the top 500 mbsf (e.g., Cook and Sawyer, 2015).

4. Results

Our depth converted seismic reflection profiles across the Bangladesh continental shelf and slope (Fig. 1) provide evidence of the presence and distribution of gas indicators within a variety of tectono-sedimentary features. Here, we first analyze the structural and stratigraphic architectural elements of the Bengal fan deposits, and then present evidence for seismic amplitude and velocity anomalies, indicative for either potential gas-bearing sediments or for BSRs in the slope domain (Figs. 2–5).

4.1. Sedimentary and tectonic features

On the continental shelf, seismic profiles show the presence of V or U-shaped profiles with an erosion surface at the bottom, filled by chaotic deposits (i.e., slumps and debrites) in their lower parts and by more well-layered high to low amplitude reflections (coarser-to finer-grained sediments, respectively) in their upper parts. Pelagic or hemipelagic drapes often characterize the topmost part of the channel/canyon infills (Fig. 2A). All these features indicate the predominance, in the shelf area, of incised channels and canyons subsequently infilled. Such sediment dispersal fairways typically develop at an early sedimentary stage due to the strong erosional ability of sedimentary flows (Sprague et al., 2005). Sediments infilling these erosional channels are also typically characterized by an overall fining upward sequence (e.g., Deptuck and Sylvester, 2018; Ma et al., 2020). Chaotic reflection packages showing contorted geometries and erosive bases, with variable internal seismic amplitude and reflection continuity representing fine-grained sediment with coarser-grained sections in some areas are also identified (Fig. 2A and 2B). These are interpreted as mass transport deposits (MTDs) (e.g., Piper et al., 1997). Channels/canyons and MTDs are embedded in low to high amplitude, parallel to sub-parallel sedimentary layers representing alternating clayey, silty and/or sandy deposits (BODC-3 Completion Report, 1978); their seismo-stratigraphic character and depositional

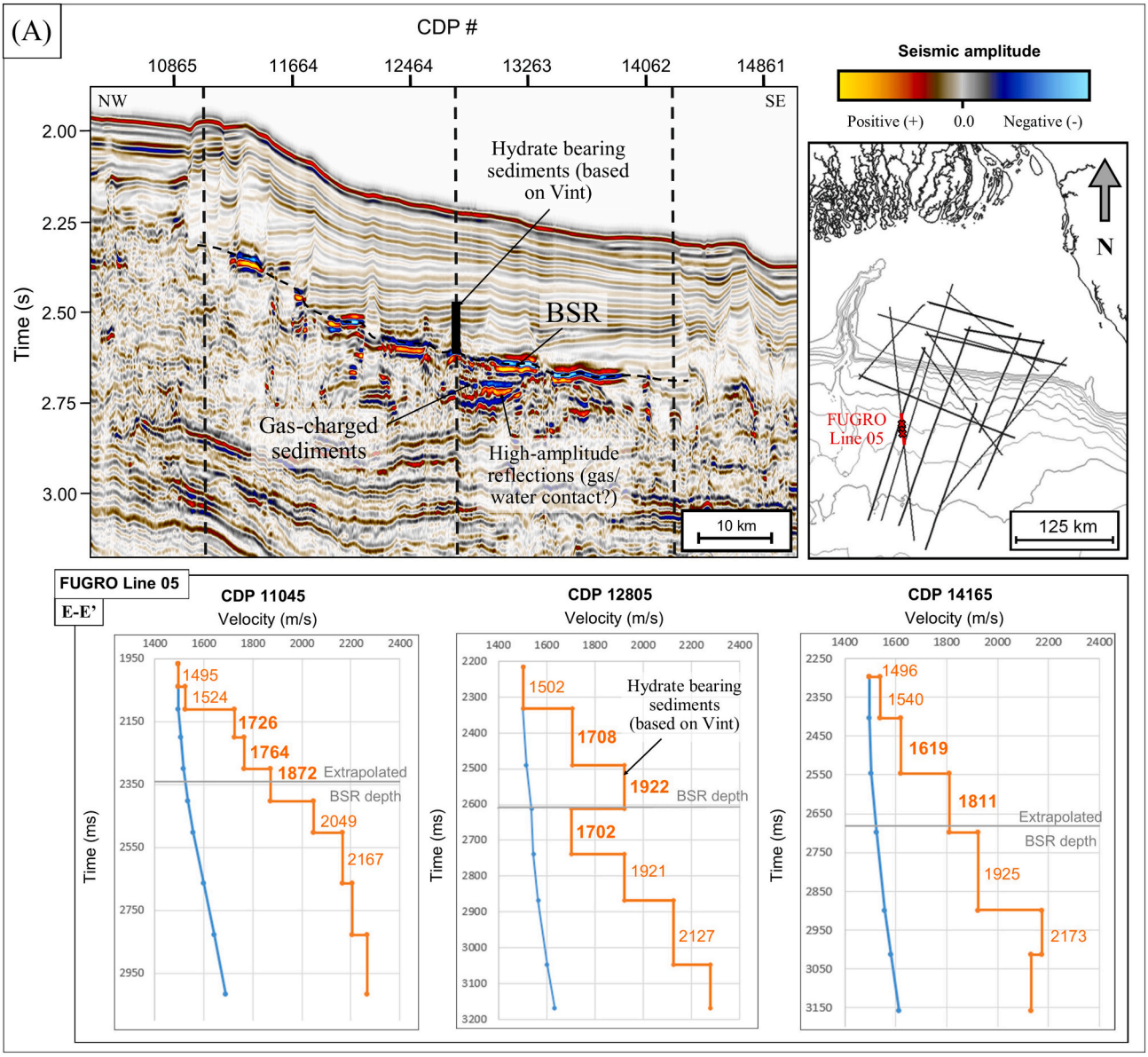

Fig. 5. Seismic profiles containing BSRs and associated 1D velocity profiles at selected Common Depth Point (CDP) locations along one FUGRO (A) and five CDF (B) profiles. Data locations are shown on inset maps: red crosses represent the 1D velocity profiles (CDPs); red segments correspond to the seismic profiles, which correspond to sections A-A′ to I–I′ in Fig. 7 and S2–S4. On 1D velocity profiles, interval velocity (V_{int}) and root-mean-square (RMS) velocity (V_{rms}) trends are shown as orange and blue lines, respectively. Horizontal grey lines represent BSR depths (in ms TWTT) at each CDP location. (For interpretation of the references to colour in this figure legend, the reader is referred to the Web version of this article.)

geometries are consistent with marine regression and transgression phases and their impact on shelf deposition and growth (Hübscher and Spieß, 2005). A few near-vertical faults are visible in the shelf domain, extending from near seafloor down to deeper stratigraphic and/or basement levels. In some cases, the faults are linked or terminate next to amplitude anomalies representing gas-charged layers (Fig. 2E).

Down the shelf break into the Bengal fan upper slope, seismic profiles reveal sediment transport and accumulation patterns related to the evolution of channelized sediment flows, which we interpret as turbidity currents. In this area, channel incision into underlying deposits is characterized by the presence, on either side of the incision, of parallel to convergent, laterally continuous reflections of low to medium amplitudes with overall wedge-shaped geometry (Fig. 2F, 2H, 2I, 3C, 4). These features are interpreted as channel-levee systems, which generally evolve from incised channels initially formed by erosion and deposition of turbidity currents leading to self-channelization and, thereafter, continuing levee building by over-spilling processes (e.g., Hiscott et al., 1997; Deptuck and Sylvester, 2018). Submarine fans may contain one main channel-levee complex or a series of channel-levee complexes that develop in succession through avulsions (e.g., Deptuck and Sylvester, 2018). In our study area, numerous cut-off loops can be observed within channel-levees (Fig. 2F). These suggest different ratios of vertical aggradation and lateral migration (Schwenk et al., 2005). Medium to high amplitude reflections dominate within the cut-and-fill deposits of the channel-levee systems, whereas well-layered, lower amplitudes often intercalated with medium-amplitude reflections, are present within the levees (Fig. 2F, 2H, 2I). Seismic evidence suggests channel cut-and-fill deposits including mostly coarser-grained sands and gravels, and levee deposits predominantly composed of finely laminated, finer-grained sediments with occasional thin sand-rich intervals,

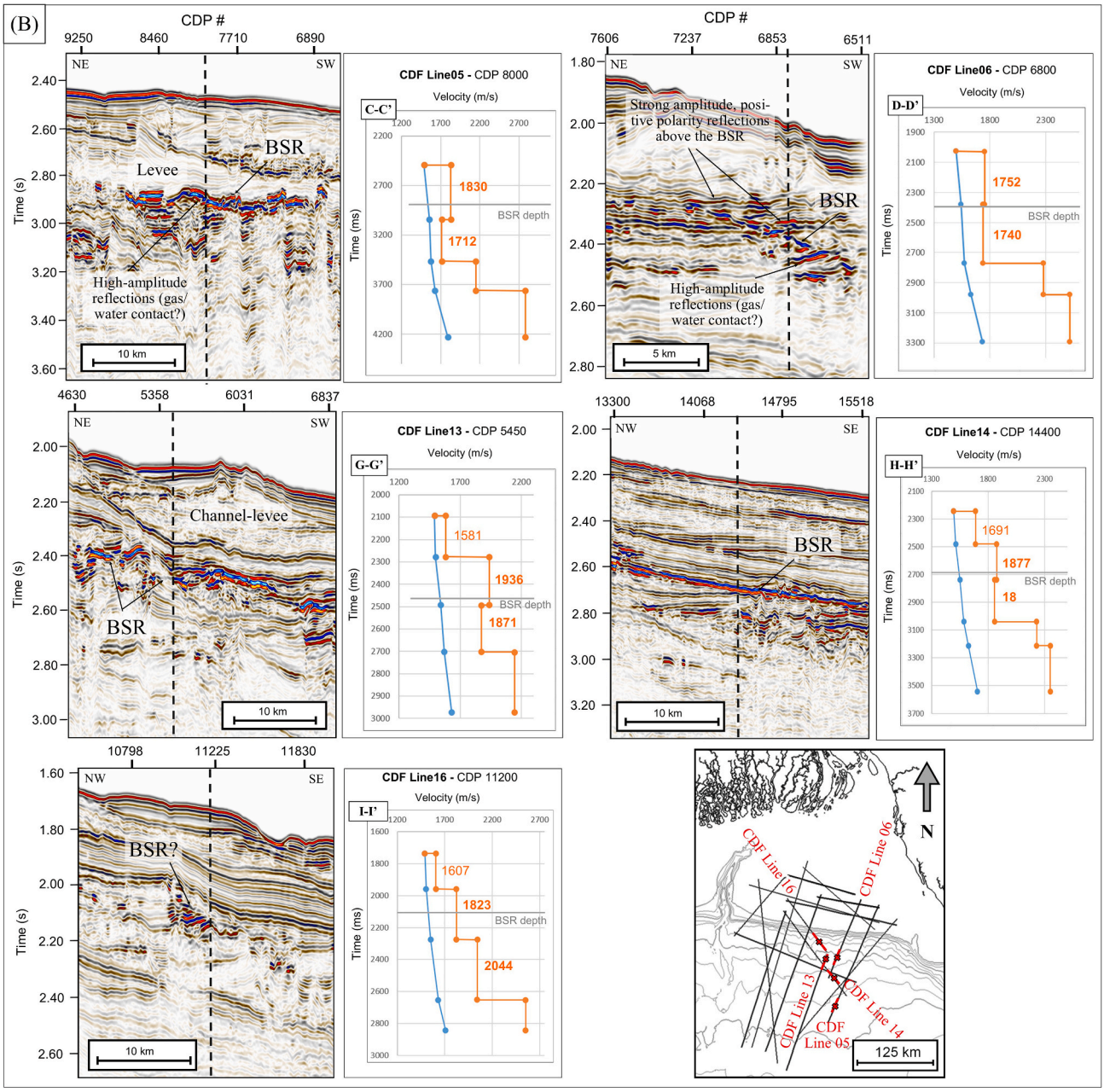

Fig. 5. (*continued*).

similarly to observations from other channel-levee areas (e.g., Hiscott et al., 1997; Deptuck and Sylvester, 2017; Shukla et al., 2019). At some locations, channel cut-and-fill units are characterized by a chaotic and high-amplitude seismic facies (Figs. 2F and 3C). These chaotic high amplitude reflectors (CHARS) are considered to represent aggraded and migrated channel axes as well as abandoned channel-fill deposits (Schwenk et al., 2005). In between channel-levee complexes, mostly parallel, sheet-like reflectors are characterized by the alternation of low/medium and high amplitude seismic facie; the latter is interpreted as beds of fine-to medium-grained sand resulting in high amplitude reflection packages (HARPS) (Fig. 2F and 2K). These are interpreted to result from levee avulsion followed by un-channelized turbidity currents flowing in intra-channel lows (Hiscott et al., 1997; Pirmez et al., 1997; Lopez, 2001; Bastia et al., 2010). Slow but continuous hemipelagic sedimentation occurring in the basin, unless remobilized by unconfined turbidite flows, may also constitute part of the sheet-like reflectors characterized by parallel and continuous, low-amplitude internal seismic facies (i.e., clay/mud) (e.g., Stanbrook and Bentley, 2022). Chaotic and low to medium reflectivity units are also visible on seismic data (Figs. 2G, 3A and 3B). These are interpreted as MTDs both embedded within sub-seafloor sediments, or as slump and sedimentary waves features at the seafloor in proximity to the steep continental slope. The latter directly affect seafloor topography, indicating recent events of slope failure and downslope sediment transfer, which may be driven by eustatic variations and/or tectonism, but that may also be triggered by gas hydrate dissociation (e.g., Nixon and Grozic, 2007).

Seismic evidence for fault and fracture systems are widely distributed in the slope area (Figs. 2H and 4), clearly revealed by coherency attributes (Fig. 4D). These systems primarily affect sedimentary units up to 1000–1200 mbsf depth, but some faults extend to greater depths (Figs. 3 and 4). Some of the shallow faults and fractures reach seafloor or near seafloor depths (Fig. 4D). Seismic signal blanking and/or disturbance effects are visible along some faults and are interpreted as evidence for active fluid migration. At seafloor depths greater than 2250 m,

at the edge of our study area, sub-circular depressions are visible at the seafloor, which are interpreted as seafloor pockmarks (Fig. 2K). These seafloor features are underlain by chimney structures, consistent with the escape of fluids to form depressions (e.g., Judd and Hovland, 1992).

4.2. Gas indicators and BSRs

Within the shelf deposits, there is evidence for widely distributed seismic amplitude anomalies typically associated with localized free gas accumulations (e.g., Judd and Hovland, 1992; Liner and McGilvery, 2019) (Fig. 2C–2E). Seismic profiles show that some anomalies are localized in small pockets (bright spots), whereas others are more laterally continuous, high reflectivity layers that suggest gas accumulation at the transition between high-permeability, high-amplitude coarse-grained sediments, and low-permeability, low-amplitude finer-grained sediments (Fig. 2C–2E). Both types of amplitude anomaly commonly lie at or near the seafloor, and are associated with seismic signal blanking, chaotic facies, and/or velocity pull-down effects beneath them (Fig. 2C–2E). Vertical or near-vertical zones with lower reflection strength than the surrounding sedimentary reflectors are interpreted as gas chimneys, and so pathways for the upward migration of fluids (Judd and Hovland, 1992) (Fig. 2D). Signal blanking and velocity pull-down effects along fault planes are interpreted as indication of fluids, likely including thermogenic gas, using the fault as a migration pathway from deeper reservoirs towards upper stratigraphic levels (Fig. 2E).

Within the deposits of the slope domain, high amplitude, negative polarity reflections (bright spots) indicate the presence of gas-bearing zones (Fig. 2H–2J). Their appearance is enhanced by seismic amplitude attributes (Fig. 4B and 4C). Some of these bright spots are underlain by signal blanking effects that may arise from signal attenuation by the gas charged layer and by chaotic facies (Figs. 2J and 4), which may be caused by disrupted sedimentary fabric due to gas migration through a fracture network (e.g., Judd and Hovland, 1992). Seismic observations indicate the presence of gas and gas migration pathways and provide indirect evidence for the potential presence of gas hydrate accumulations in this area.

In the slope region, within a water depth range of 1300–1900 m, seismic reflections of variable continuity that parallel the seafloor at sub-seafloor depths of several hundred meters are observed, showing high amplitudes with reversed polarity, and crosscutting the background stratigraphy (Figs. 3 and 5). Such reflections are interpreted as BSRs, likely representing the BGHSZ (e.g., Kvenvolden and Barnard, 1983; Hyndman and Spence, 1992).

Seismic attributes enhance the amplitudes associated with the BSR (Fig. 4B and C). In some places, beneath the BSR, high amplitude layers are observed (Figs. 3 and 4). These layers show a strong negative polarity reflection followed by a strong positive polarity reflection, and they generally lie sub-parallel to the BSR or are dipping to terminate against it (Figs. 3, 4B and 4C, 5). Strong positive polarity reflections may arise at gas-water interfaces (e.g., Judd and Hovland, 1992; Portnov et al., 2021) and could, therefore, be associated with the base of an interval containing free gas trapped beneath the BGHSZ.

Mapping of the BSR shows it is predominantly located towards the E-SE of the Bangladesh EEZ, in water depths of 1300–1900 m and at depths below seafloor of 250–440 m (Fig. 6). The BSR is often discontinuous and observed on seismic profiles over distances of up to 100 km (i.e., CDF Line 14), which in map view form several areas of varying size (Fig. 6). Fault and fracture systems affect BSR continuity at several locations where they crosscut and/or terminate at the base of the BSR (Fig. 3A, 3C, 4). Where faults/fractures terminate at the base of the BSR, they are sometimes associated with abrupt terminations of high amplitude reflections (Figs. 3 and 4). In places, bright spots are visible above the BSR, and are associated with gas accumulations that attenuate the seismic signal and generate blanking effects that obscure the subjacent stratigraphy (Figs. 2J, 3C and 4).

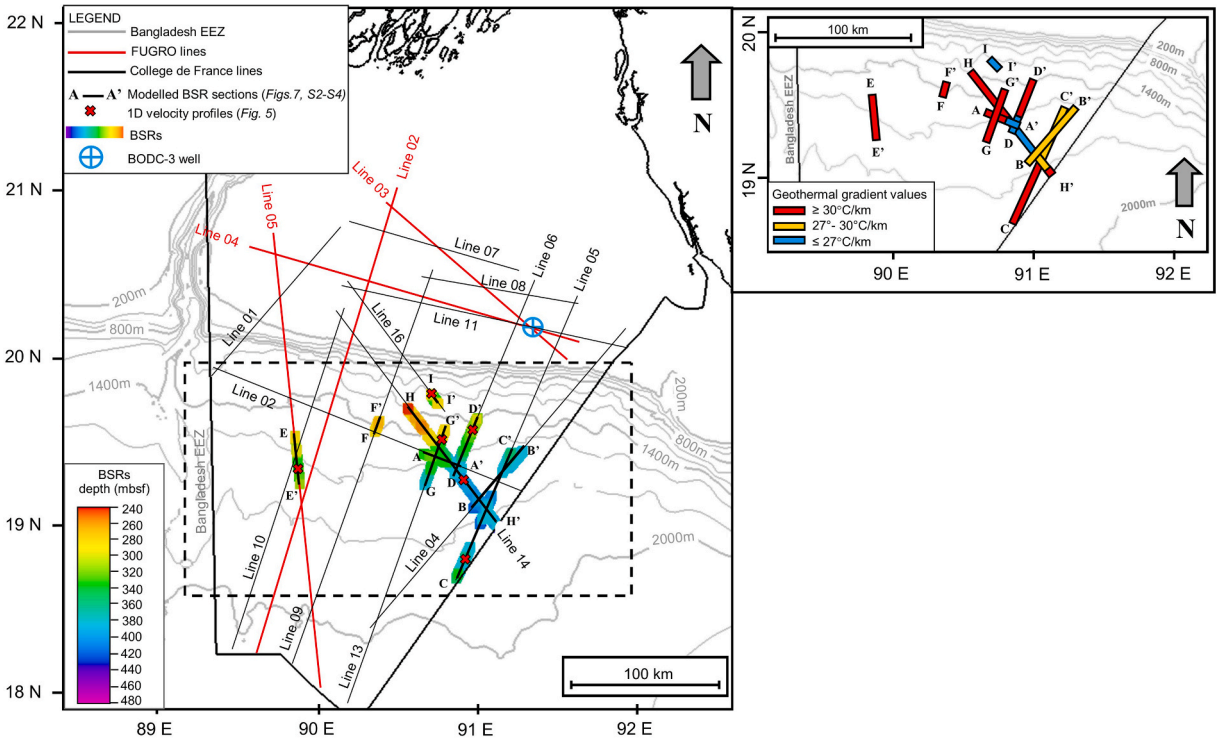

Fig. 6. Map showing the distribution of BSRs and their depth in meters below seafloor (mbsf). Contour interval in map is 200 m. Black segments (A-A′ to I–I′) refer to the seismic examples in Fig. 5 and to the modelling results in Fig. 7. Red crosses refer to the velocity profiles in Fig. 5. Dashed box refers to zoomed map (top right) displaying geothermal gradients distribution based on BGHSZ modelling results. (For interpretation of the references to colour in this figure legend, the reader is referred to the Web version of this article.)

4.3. Interval velocities across BSRs

Stacking velocities provide average interval velocities for sediments down to 500 mbsf, which is near the maximum depth (440 mbsf) at which BSRs are observed. Sediments outside the interpreted BSR areas show average interval velocities between ~1600 m/s and ~1870 m/s over this depth range (Fig. 5). Sediments above BSR locations generally show higher interval velocities reaching values of ~1920–1940 m/s (Fig. 5). Higher average interval velocities within the BSR areas are consistent with the presence of gas hydrate in shallow marine sediments (Singh et al., 1993; Helgerud et al., 1999; Riedel et al., 2014).

Interval velocities from seismic data (observed velocities) can be compared with those calculated from rock physics models to estimate ranges of hydrate saturation within sediments, based on the best-fitting parameters. Using the Marín-Moreno et al. (2017) model and assuming a sand/quartz-dominated sediment frame with a bulk modulus of 36 GPa and a shear modulus of 45 GPa, a 30% sediment porosity, and methane hydrate-forming gas composition, we find that the interval velocities observed in sediments above the BSR can be explained with a gas hydrate saturation of less than about 5% depending on hydrate habit. The accuracy of the gas hydrate saturation depends on the accuracy of the interval velocities, as the saturation of the different pore phases are calibrated to fit the 'observed' P-wave velocities. The interval velocities have low resolution, and hence the value of 5% gas hydrate saturation should be interpreted qualitatively as an indicator of low hydrate saturation in the system.

Decreases in interval velocity from 1900 m/s to 1700 m/s (corresponding to a 220 m/s decrease in interval velocity) are observed beneath the BSR in some places (Fig. 5A). This low-velocity zone is often associated with high amplitude reflections that lie subparallel to the BSR or terminate against it (Figs. 3–5). The decrease in interval velocities, together with the presence of high amplitude, negative polarity reflections, are consistent with the presence of free gas beneath the BGHSZ. Beneath this free gas zone, high-amplitude, positive polarity reflections are attributed to gas-water interfaces within stratigraphic layers underlying the BGHSZ (e.g., Judd and Hovland, 1992; Andreassen et al., 1997; Chabert et al., 2011; You et al., 2019).

At some locations, velocity inversions beneath the interpreted BSR are less pronounced, and interval velocities for sediments above the BSR fall within the range for potentially non-gas hydrate-bearing sediments (Fig. 5B). Lateral variations in interval velocity along the interpreted BSRs may reflect changes in the saturation of hydrate within the sediments (e.g., Chabert et al., 2011). However, as velocities available for this study have a relatively coarse vertical resolution (~100 ms; Fig. 5), they may only represent averages of consecutive high- and low-velocity intervals. Nevertheless, BSRs and associated seismic velocities seem to indicate either the occurrence of overlying gas hydrate-bearing sediments showing higher interval velocities, or the presence of underlying free gas-bearing sediments showing lower interval velocities, or both (e.g., Gullapalli et al., 2019). To further support the hydrate-related nature of the identified BSRs, we compare the modelling of the BGHSZ with our seismic observations.

4.4. Modelling of the BGHSZ

We tested several models using different geothermal gradients between 25 °C/km to 30 °C/km and positive perturbations of seafloor temperature of up to 3 °C relative to the NOAA data-derived profile (Figures S1). Our results show that with the NOAA data-derived temperature profile (Figure S1), a 25 °C/km to 27 °C/km geothermal gradient (Akbar, 2011) gives a BGHSZ much deeper than the seismically identified BSRs and outside their depth error estimates (Figure S2). A geothermal gradient of 27 °C/km to 30 °C/km (Guha et al., 2010) provides a better fit between the calculated BGHSZ and BSRs, particularly a value of 30 °C/km (D; H–H'; I–I' - Figure S2). Higher values are not reported in the Bangladesh offshore area and would result in a BGHSZ shallower than the seismically identified BSRs. We therefore set a 30 °C/km geothermal gradient as a reasonable parameter for the modelling. The calculated BGHSZ nonetheless remains deeper than the interpreted BSRs along some profiles (i.e., A-A'; B–B'; C–C'; D'; E-E'; F–F'; G-G'; Figure S2). On most profiles, a better fit is obtained by assuming a seafloor temperature increase between 2 °C and 3 °C (Figures S3, S4). Our selected model therefore uses a geothermal gradient of 30 °C/km and a seafloor temperature 2.5 °C greater than NOAA data (Fig. 7), although we do not exclude that temperatures may vary along the seismic profiles.

5. Discussion

5.1. The Bangladesh gas hydrate system

Our seismic profile show the morphology of the upper Bengal fan delta front to exhibit an alternation of channel-levees, over bank deposits, mass-transport deposits (MTDs), and irregular features formed by sliding/slumping (Figs. 2–3). We interpret the turbidites to result from confined flows in channel-levee complexes, recorded by fining upward patterns within the channel infill (Fig. 2F and 2I), whereas thin sand-shale alterations are more common in the levees and over bank deposits (Fig. 2F, 2H, 2IF, H, 2I). Tabular-bedded deposits, indicated as HARPS, are interpreted to record unconfined flows (i.e., flows not confined by levees) (Fig. 2F and I).

The identification of BSRs in this depositional setting provides insights into the presence and distribution of the natural gas hydrate system in the northern BoB (Fig. 6). BSRs are observed within slope deposits at depths of 250–440 mbsf, in water depths of 1300–1900 m (Fig. 6). Slope deposits show an alternation of low and high amplitude reflections interpreted as interbedded sequences of sand, silt, and clay layers, mostly associated with turbidites and channel-levee deposits (Figs. 3 and 4). Although both coarse- and fine-grained intervals may contain gas hydrate, coarse-grained sediments (i.e. sands) generally show the highest gas hydrate saturation potential (e.g., Ginsburg et al., 2000; Boswell and Collett, 2006; Torres et al., 2008; Riedel et al., 2013a, b; Collett et al., 2014; Max and Johnson, 2014). BSRs in the Bangladesh EEZ are predominantly associated with high-amplitude, sheet-like deposits, which we interpret to record deposition during un-confined flows resulting from channel avulsion and/or turbidity current over-flow (HARPS; Figs. 2H and 3), and with channel cut-and-fills deposits (Fig. 2I). MTDs identified within the slope region may have also played an important role in controlling the gas hydrate-bearing sediments. This is because MTDs provide a rapid accumulation of sedimentary material, which can contribute to changes in the thermal regime of the sub-seafloor sediments. Following these changes, the GHSZ will try to re-equilibrate to the new thermal structure making the BGHSZ to move upwards (e.g., Mandal et al., 2014).

Along east Indian margin most gas hydrate occurrences are also associated with deep-water fan deposits (i.e., channel-levee systems) likely to be sand prone reservoirs systems (Collett et al., 2019; Holland et al., 2019). Offshore Myanmar, drilling at the Shew gas field (Fig. 1) indicates hydrocarbon accumulations mainly within the distal lobe deposits (end of channel systems) formed by sandy turbidites (Yang and Kim, 2014); these sandy turbidites are capped by fine-grained (i.e., muddy) hemipelagic deposits, acting as an effective trap for hydrocarbon accumulation (Zhan et al., 2019).

Given the proximity and similarity of the Myanmar and eastern India depositional settings with the Bangladesh EEZ, and based on BSRs distribution on seismic data, we infer that coarse-grained deposits associated with confined (channel systems) and un-confined (i.e., turbidite) flows are the most likely to host gas hydrate accumulations within the Bangladesh EEZ.

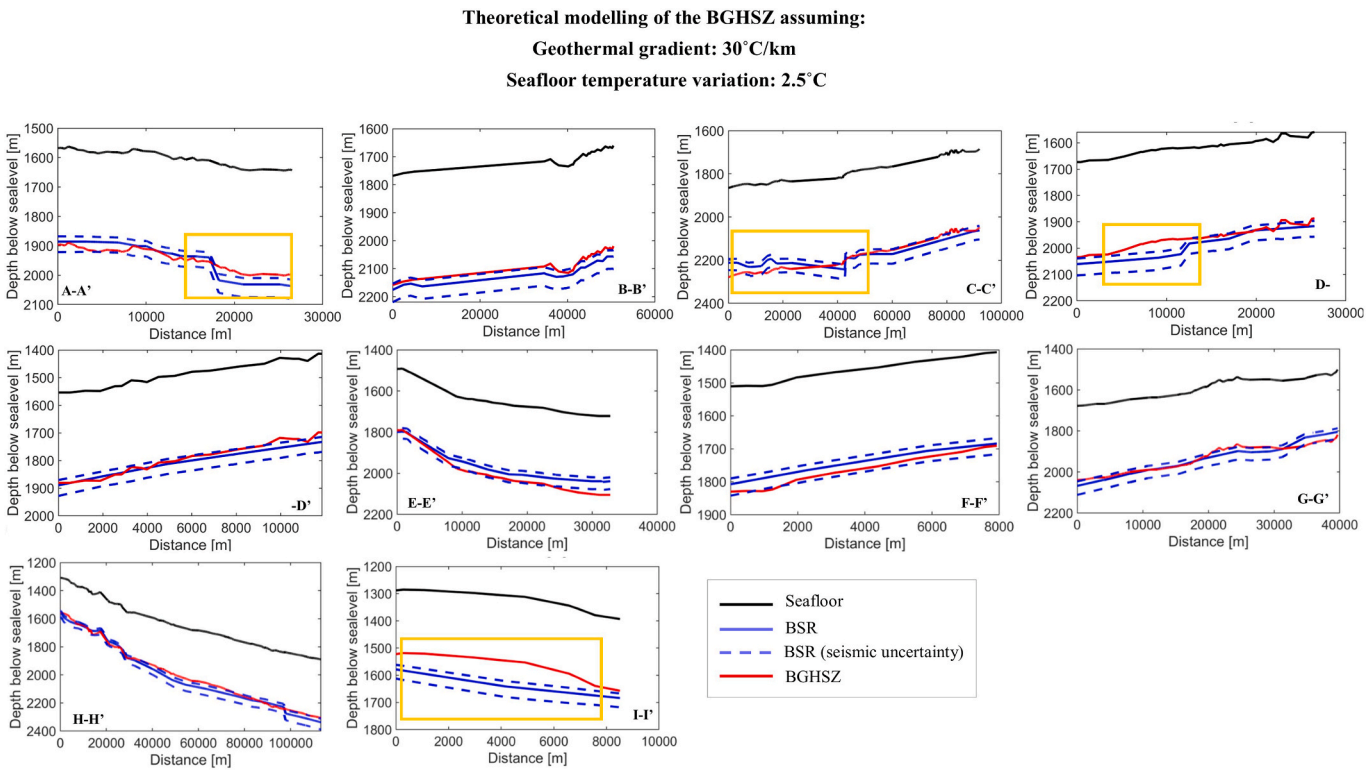

Fig. 7. Plots comparing the observed BSRs with results from the theoretical modelling of the BGHSZ assuming 100% methane gas composition, 3.5 % wt pore water salinity, 30 °C/km geothermal gradient, and a 2.5 °C increase in seafloor temperature relative to NOAA-derived temperatures (https://www.nodc.noaa.gov/OC5/woa18f/). Plot locations are shown in Fig. 6 (segments A-A′ to I–I′). Note that segment D-D′ is divided in two plots (D- and -D′) representing adjacent portions of CDF Line 06. Black lines represent seafloor depth along seismic profiles; continuous blue lines are observed BSR depths, and dashed blue lines show BSR depth variation for a −100 m/s decrease and a +200 m/s increase in interval velocities used for time-depth conversion; red lines represent the calculated BGHSZ. Yellow boxes highlight areas where an offset exists between the BSR and the calculated BGHSZ (see Fig. 8). (For interpretation of the references to colour in this figure legend, the reader is referred to the Web version of this article.)

5.2. BSR character and discontinuity

The BSRs identified offshore Bangladesh (Fig. 6) are variable in reflection strength and lateral continuity (Figs. 3 and 4). The seismic expression of a BSR can be controlled by many factors and may, for instance, result from the way in which gas hydrate forms and accumulates within a specific interval (e.g., Shukla et al., 2019), which in turn can be controlled by the way in which gas migrates into the GHSZ (You et al., 2019). For instance, dissolved methane is not sensitive to the capillary entry pressure of the hosting media either to eventual reductions of permeability induced by multi-phase flow and hydrate formation (Bear, 2013), and can migrate in solution until super-saturation induces its exsolution to form free gas accumulations or gas hydrates (Liu and Flemings, 2007). Migration in solution, therefore, likely creates a more homogeneous and laterally continuous distributions of gas hydrate within the GHSZ which may, in turn, result in a more continuous character of the BSR (Foschi et al., 2019). However, the presence of a continuous BSR (Fig. 3C) could also be an indicator of free gas being dispersed in the pores below the BGHSZ, rather than the presence of significant gas hydrate above it (e.g., Holbrook et al., 1996; Max and Johnson, 2014).

When methane migrates in gas phase it may be restricted to pathways with sufficiently large pores and low capillary entry pressures, allowing pore invasion and displacement of the resident pore water (e.g., Fauria and Rempel, 2011). Migration across low-permeability formations may still occur, but it would require gas overpressure able to breach eventual sealing units and form fractures (Cartwright and Santamarina, 2015). Essentially, the focused distribution of available free gas and migration pathways will control the eventual distribution of gas hydrate (e.g., Hillman et al., 2017; You et al., 2019), and may result in a more discontinuous character of the seismic BSR (e.g., Hustoft et al., 2007; Shedd et al., 2012). Although our observed BSRs are quite discontinuous or even absent in places (i.e., Figs. 3A and 3B, 4), their absence does not rule out the presence of gas hydrate which may be present at low saturations (e.g., Chabert et al., 2011).

Active fluid flow through the GHSZ (e.g., Ramana et al., 2006), often associated with the presence of active faulting (e.g., Fichler et al., 2005), can also have a strong impact on BSR continuity. Our seismic data show that fault and fracture systems reach and crosscut the GHSZ, sometimes also acting as conduits for the migration of fluids from deeper stratigraphic levels (Figs. 3 and 4). Deep fluid sourcing may be evidenced by the presence of low-velocity zones (Fig. 5) indicating free gas trapped beneath the BGHSZ by overlying gas hydrate-bearing sediments of low permeability (e.g., Wang et al., 2020). Gas-charged sediments and gas-water contacts can explain the presence of high amplitude reflections beneath the BSR (e.g., Judd and Hovland, 1992) (Figs. 3–5). Elsewhere, fluids entering the GHSZ via faults or fractures may continue migrating at rates too great to allow gas hydrate formation due to reaction kinetics (e.g., Fauria and Rempel, 2011), thus having an impact on hydrate equilibrium conditions.

Lateral variations in the BSR strength and continuity may also result from local perturbations of the gas hydrate stability field (e.g., Shukla et al., 2019). The presence of gas within the GHSZ is indicated by amplitude anomalies that partly or entirely obscure the BSR, which are observed in the shallower areas of its occurrence in water depths of 1300–1500 m (Figs. 3C and 4). The feather edge of the GHSZ, where the base GHSZ lies within tens of meters of seafloor, is considered to be more sensitive to climate-driven factors that may change stability conditions, such as sea level variations and sedimentation rate (Ruppel, 2011). In such a setting, gas hydrate dissociation may result in the release of gas

and its migration to seafloor (e.g., Ketzer et al., 2020). However, our shallowest BSR lies at water depths around 1300 mbsl and depths ≥250 mbsf (I–I′, Fig. 6), and so is unlikely to have been affected by such factors (Ruppel and Kessler, 2017). In the same areas, the presence of seafloor MTDs may be an evidence of past gas hydrate dissociation and/or rapid migration of methane through faults and fractures to induce slope failure (Fig. 3B). Gas hydrate dissociation can increase local pore fluid pressure in sediment, depending on the ratio of fluid pressure dissipation to fluid release from dissociation, decreasing the effective normal stress and shear resistance (e.g., Hornbach et al., 2004), or ultimately triggering sediment collapse (De La Fuente et al., 2020).

5.3. Seismic velocities across the BSRs

Seismic velocities can help to discriminate the nature of the acoustic impedance contrasts generating BSRs. In the Bangladesh offshore, interval velocities show that the BSR corresponds, in general, to the base of a higher velocity layer, indicating the likely presence of gas hydrate-bearing sediments (Fig. 5). Interval velocities from sediments outside interpreted BSR areas are generally lower and are presumably linked to non-gas-hydrate-bearing sediments (Fig. 5A). Beneath most areas of the BSR, a decrease in interval velocities is consistent with sediments that do not contain gas hydrate, but most likely contain free gas trapped beneath the GHSZ (Fig. 5). At some locations, the absence of a velocity increase above the BSR (i.e., D-D′, H–H′, I–I' - Fig. 5B) suggests either an absence of gas hydrate, or that the saturation of hydrate is too low to be resolved (Chabert et al., 2011). Considering the coarse vertical resolution of the interval velocities available for this study (~100 ms), values for the BGHSZ may be an average of higher velocities due to gas hydrate above and lower velocities due to gas below, thus explaining the absence of an increase above the BSR (e.g., D-D′, H–H′, I–I' - Fig. 5B). Gas hydrate may also have a patchy distribution, but lateral variations in interval velocities along sedimentary layers are poorly constrained by wide picking intervals (i.e., 5 km along CDF lines).

Gas hydrates can occur anywhere within the GHSZ, but commonly show a heterogeneous distribution depending on the availability of hydrocarbon gas and pore water, salinity, permeability, porosity, etc. (e.g., Duan et al., 2011; Klauda and Sandler, 2005). At a given location, the top and bottom of the potential zone of gas hydrate occurrence are controlled by the gas (methane) solubility in the pore space and the availability of gas (Ruppel and Kessler, 2017). The top of the gas hydrate occurrence zone (e.g., Riedel and Collett, 2017) may be indicated by an increase in interval velocities, but it is not possible to recognize this offshore Bangladesh due to the low vertical resolution of seismic interval velocities. Another possible indication for the extent of the hydrate-bearing sediments is the presence of high amplitude, positive polarity reflections above the BSR (e.g., Posewang and Mienert, 1999). Strong reflections are observed above the BSR on CDF Line 06 (D-D'; Fig. 5B), but nowhere else on our seismic data. The lack of strong reflections within the GHSZ may be due to a low (less than 5%) gas hydrate saturation in sediments, as estimated from seismic velocities.

Beneath the BSR, the presence of free gas offers the most plausible explanation for the observed low-velocity zone corresponding to a decrease in P-wave velocities (Fig. 5). The presence of free gas can also explain the high-amplitude reflections, characterized by a negative acoustic impedance contrast followed by a positive acoustic impedance contrast, visible beneath the BSR, which often terminate against it (Figs. 4 and 5); these sub-parallel or dipping reflections may indicate the gas hydrate-free gas and free gas-water interfaces beneath the BGHSZ, respectively (Judd and Hovland, 1992).

Although seismic velocities support their gas hydrate-related nature, the identified BSRs show a variable seismic character and distribution across the study area. This variability is further assessed comparing seismic observations with numerical modelling for the BGHSZ.

5.4. Theoretical BGHSZ

The depth of the interpreted BSR generally shows a good match with the calculated BGHSZ, further supporting the gas hydrate-related nature of the BSR (Fig. 7). However, clear offsets are observed in some lines (yellow boxes - Fig. 7).

The offsets between observed BSRs and calculated BGHSZ cannot be related to seismic picking errors along the BSR, as this is estimated to be within a maximum of 8–15 m (distance from top to bottom of the negative peak along which the BSRs are interpreted). These offsets may be related to uncertainty in choosing model parameters for the calculated BGHSZ. Assuming a constant 2.5 °C seafloor temperature increase, model fit is improved by using a 27 °C/km instead of a 30 °C/km geothermal gradient at some locations (Figure S4). BSRs in the E-SE part of the study area are best-fit by a BGHSZ calculated assuming a 27 °C/km geothermal gradient, or by an intermediate geothermal gradient between 27 °C/km and 30 °C/km (Fig. 6; Figure S4). BSRs in the central and W-NW area are instead best-fit assuming a geothermal gradient ≥30 °C/km (Fig. 6; Figure S4). This suggests that geothermal gradient may vary up to 3 °C/km, with higher values to the W-NW and lower values to the E-SE part of the Bangladesh EEZ (Fig. 6). A similar spatial trend was inferred from down-hole temperature measurements along the shelf domain (Guha et al., 2010). However, along-slope variation in geothermal gradients does not explain the observed sudden changes in BSR morphology, including vertical offsets (of up to 100 m) which do not follow seafloor topographic trends (i.e., A-A'; C–C'; D-; Fig. 7).

The depth of the BSR can be influenced by several mechanisms that affect the thickness of the GHSZ, including sediment type (i.e., texture, mineralogy, and porosity) and salinity (e.g., Clennell et al., 1999; Sahoo et al., 2018). Nucleation kinetics of gas hydrate and/or of free gas bubbles may be inhibited by confinement of the methane-bearing fluid in small pores, and equilibration may also be limited by rates of diffusion of gas, water, and salt components or by advective flows of fluid or heat (e.g., Henry et al., 1999). However, local variations in salinity and/or pore-size produce only moderate shifts in the position of the gas hydrate stability field (e.g., Milkov and Sassen, 2001; Foschi et al., 2019), which cannot explain vertical shifts of up to 100 m as observed in our data (i.e., A-A'; Fig. 7).

The depth of the BGHSZ is sensitive to both thermal perturbation and to changes in the hydrate-forming gas composition (e.g., You et al., 2019). Most observed offsets between the BSR and the calculated BGHSZ are close to fault/fracture systems, often associated with evidence for fluid migration (Figs. 7 and 8). Fluid migrating through fault systems can be associate with the transport both of heat (e.g., Sain et al., 2011; Shedd et al., 2012), and of deeply sourced thermogenic gases (e.g., Kvenvolden, 1993).

In areas where the BSR is shallower than the BGHSZ (C–C'; Fig. 7), the upward shift may be due to warm fluids rising along faults/fractures observed on seismic data (C–C'; Figs. 7 and 8). However, in most locations BSRs lie deeper than the calculated BGHSZ (A-A′, D-, I–I'; Fig. 7), and are also characterized by the presence of deep fault systems terminating at the BSR or crossing the GHSZ (A-A′, D-, I–I'; Fig. 8). At these locations, the deepening of the BSR could be explained by the presence (even in small amounts) of heavier molecular hydrocarbons (e.g., Collett et al., 2009; Sloan and Koh, 2008; You et al., 2019). Heavier molecular hydrocarbons originating at depth may migrate upwards through focused pathways such as faults and fractures, or simply via diffusion through permeable layers, and increase the thickness of the GHSZ (e.g., Hillman et al., 2017). The presence of deep faults (>1 km bsf; Fig. 4D) reaching and crosscutting the GHSZ and the seismic evidence for fluid flow along them, together with the presence of low-velocity zones associated with high amplitude seismic anomalies sub-parallel or dipping and terminating against the BSR (Fig. 5), are strong indicators for the existence of a deeper, thermogenic gas (e.g., Hillman et al., 2017; Shukla et al., 2019). Along the east Indian continental margin, seismic data have revealed the presence of faults extending from the near

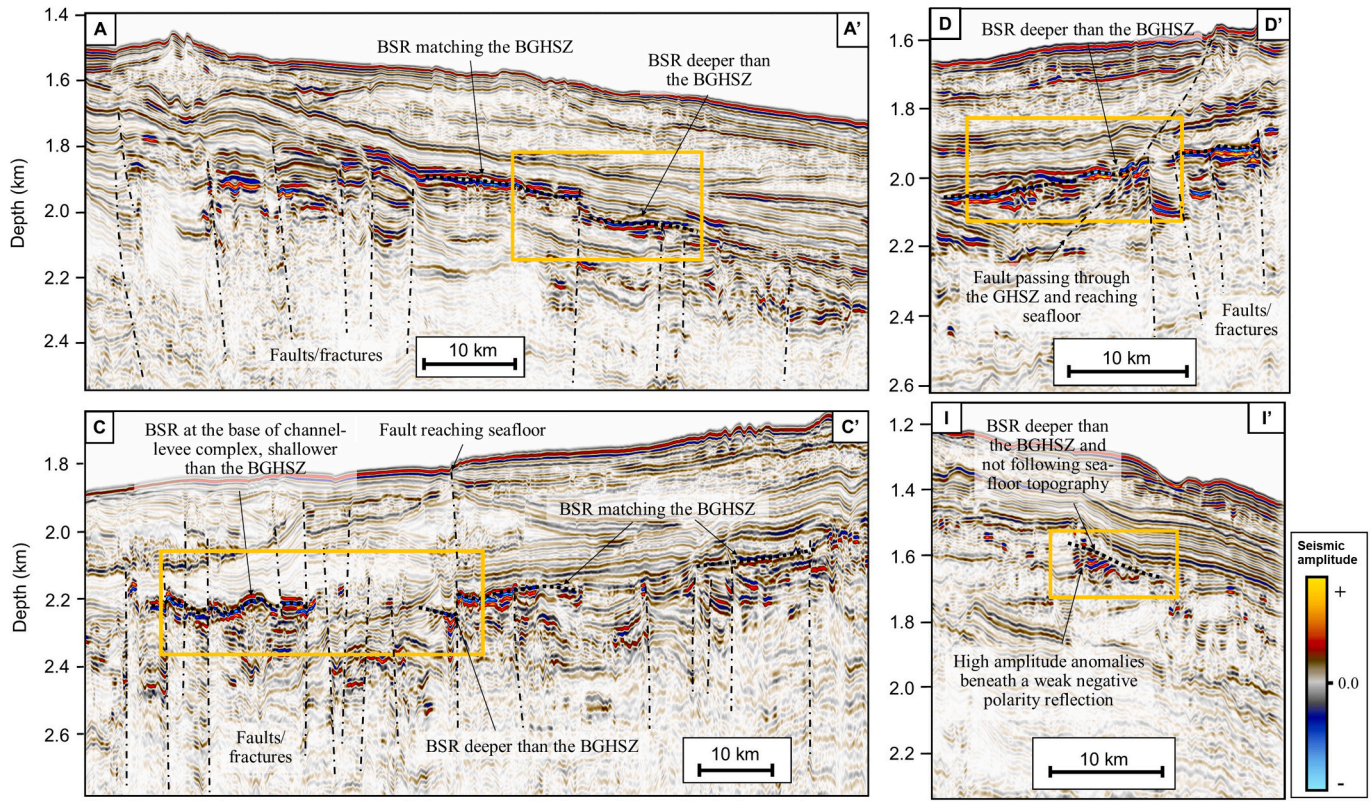

Fig. 8. Seismic profiles including segments A-A' (CDF Line 02), C–C' (CDF Line 05), D-D' (CDF Line 06), and I–I' (CDF Line 16) (segment locations are shown in Fig. 6). Yellow boxes highlight areas where the BSR (black dotted lines) shows vertical shifts from the calculated BGHSZ (cf. Fig. 7). Fault/fracture systems affect BSR continuity in these areas (i.e., A-A′). Upward migration of deeply sourced fluids along the faults can shift the BGHSZ upward or downward (i.e., C–C'; D-D′), where warm fluids or heavier hydrocarbons enter the GHSZ, respectively. In (I–I′), free gas beneath the potential gas hydrate-bearing region may be indicated by the presence of high amplitude layers abruptly terminating against a weak, negative polarity reflection interpreted as a BSR. (For interpretation of the references to colour in this figure legend, the reader is referred to the Web version of this article.)

surface to approximately 2000 mbsf within the expected temperature zone of thermogenic hydrocarbon generation; these faults may have acted as conduits for thermogenic gas migration from deep to shallow levels (e.g., Dewangan et al., 2011).

Studies in diverse geological settings containing gas hydrate have indicated contributions from both microbial and thermogenic methane (e.g., Bourry et al., 2009; Kroeger et al., 2015; Dumke et al., 2016; Hillman et al., 2017; Minshull et al., 2020). A recent study in the Gulf of Mexico has shown that a gradual change in gas mixtures (from thermogenic to microbial sources) may influence the thickness of the GHSZ, and result in non-seafloor parallel BSRs (Portnov et al., 2021). Previous work suggests that the gas hydrate system we identify offshore Bangladesh is also likely to be characterized by mixed gas compositions. Methane concentrations related to bacterial methanogenesis and bacterial oxidation have been detected offshore Bangladesh in surface waters and in continental shelf deposits close to the Ganges-Brahmaputra mouth (Berner et al., 2003). In addition, studies on gas seeps onshore and offshore Bangladesh have shown that, with exception of small bacterial contributions in some surface seep gases and two subsurface accumulations, the gas is predominantly thermogenic (including higher molecular hydrocarbon gases i.e., ethane, butane) sourced at peak generation depths of at least 6 km within Miocene formations (Curiale et al., 2002). Several thermogenic gas sources may be available in this area, as supported by the existence of deep hydrocarbon systems offshore Bangladesh (Eocene-Oligocene age; Imam and Hussain, 2002), and by reports coming from onshore and offshore exploration wells of commercial discoveries of natural gas in sandstones of the Miocene-Pliocene Surma Group (i.e., Sangu and Kutubdia gas fields; Imam and Hussain, 2002) (Fig. 1). Deeply sourced thermogenic gas may have migrated through faults and/or permeable layers accumulating within shallower sedimentary units. Gas accumulations at different depth in sediments of the Bangladesh continental shelf is reported in the BODC-3 exploration well (Figs. 1 and 6), and correlated to bright spots at depths between 1000 and 2400 m bsf (BODC-3 Completion Report, 1978).

Based on the above evidence, we suggest that localized fluid flow through faults/fractures may explain the offsets that we observed between the BSR and the calculated BGHSZ (Fig. 7). We recognize that gas hydrate stability may also be influenced by variations in heat-flow that depend on rates of sedimentation as well as sediment type (Hutchison, 1985), different lithologies having different thermal conductivity. However, localized changes due to fluid flow through structural elements (faults/fractures) are considered to have a primary control on heat flow in the near-surface sediments of the study area. The rise of warm fluids through fault and/or fracture systems can explain observed BSRs shallower than the modelled BGHSZ (i.e., left end-side of C–C'; Figs. 7 and 8). A similar finding is available from the east Indian margin, where fault and fracture systems related to neo-tectonic activity have been estimated to generate a 15–20% increase in heat-flow due to the upward migration of deeply sourced fluids, influencing the distribution of gas hydrates (Dewangan et al., 2011). In addition, offshore Bangladesh, the supply of thermogenic hydrate-forming gases through fault and/or fracture systems, can explain observed BSRs deeper than the modelled BGHSZ (i.e., A-A′, D-D′, I–I'; Figs. 7 and 8).

Our results show the complexity of the gas hydrate system identified in the Bangladesh EEZ and highlights the need for further data to better understand the mismatches between seismic observations and modelling results. New surveys should consider the acquisition of 3D seismic

reflection data, particularly focusing on the E-SE part of the study area where several BSRs have been identified along the CDF profiles (Fig. 6). 3D imaging at this location would provide better constraints on the spatial distribution and character of the gas hydrate accumulations, and their interaction with tectono-stratigraphic elements in the area. In addition, coring, drilling and downhole logging of physical properties (i.e., electrical resistivity, formation densities, sonic velocities, etc.) at selected locations would help to define the composition, saturation and thickness of the gas hydrate-bearing sections. As a priority location, coarse-grained beds associated with both confined and un-confined turbiditic flows seem to offer the most promising locations for gas hydrate reservoirs within the Bangladesh EEZ. The acquisition and integration of such data would help to guide the identification and characterization of gas hydrate-bearing sediments in order to assess potential exploitation targets in this promising, but yet underexplored, region.

6. Conclusions

This study provides on the first evidence of gas hydrate occurrence in the northern Bay of Bengal (BoB), offshore Bangladesh, and insights into the controls on its distribution and character. Seismic profiles reveal the presence of BSRs in water depths of 1300–1900 m, preferentially located in mixed-to coarse-grained deposits of the slope domain. Calculation of the stability zone for pure methane hydrate demonstrates the gas hydrate-related nature of the BSRs, with a good match between the calculated BGHSZ for a geothermal gradient of 30 °C/km, and seafloor temperatures between 2.7 °C and 5.3 °C (+2.5 °C temperature increase from NOAA-derived temperatures). Nonetheless, in many places the BSR lies above or below the calculated BGHSZ, notably in close proximity to faults and fractures systems. Based on seismic observations, we infer that faults and fractures likely act as pathways for the upward migration of deeper fluids, creating local perturbations in heat-flow and/or supplying heavier hydrate-forming gases that locally affect gas hydrate stability.

These initial results are promising in terms of the occurrence of gas hydrates offshore Bangladesh and should guide future research and exploration initiatives to identify new gas hydrate reservoirs, to better understand their spatial distribution and to quantify the total occurrence of gas hydrates in the EEZ of Bangladesh. Against the backdrop of increasing energy demand, gas hydrates represent a potential solution for the future energy security of Bangladesh.

Author statement

Vanessa Monteleone: Conceptualization, Methodology, Investigation, Visualization, Writing – original draft.; **Hector Marin-Moreno:** Conceptualization, Methodology, Investigation, Validation, Supervision, Writing – review & editing.; **Gaye Bayrakci:** Conceptualization, Investigation, Validation, Supervision, Writing – review & editing; **Angus I. Best:** Project concept and oversight, Validation, Writing – review & editing; **Farhana Shaon:** Member, Bangladesh Scientific Team, Data supply, Validation and review; **Mohammad Moinul Hossain:** Member, Bangladesh Scientific Team, Data supply, Validation and review; **Cdr. Ahmad Al Karim:** Member, Bangladesh Scientific Team, Data supply, policy intervention, Writing – review & editing; **Md Khurshed Alam:** Leader, Bangladesh Scientific Team, Data supply, policy intervention, Writing – review & editing.

Declaration of competing interest

The authors declare the following financial interests/personal relationships which may be considered as potential competing interests: Vanessa Monteleone reports financial support was provided by Government of Bangladesh, Ministry of Foreign Affairs (MOFA). Gaye Bayrakci reports financial support was provided by Government of Bangladesh, Ministry of Foreign Affairs (MOFA). Angus Best reports financial support was provided by Government of Bangladesh, Ministry of Foreign Affairs (MOFA). Hector Marin-Moreno reports financial support was provided by Government of Bangladesh, Ministry of Foreign Affairs (MOFA).

Acknowledgements

The authors are thankful to the Bangladesh Ministry of Foreign Affairs (MOFA) for sponsoring and contributing to this study, and to Petrobangla and Bangladesh Petroleum Exploration & Production Company (BAPEX) for making available the seismic reflection data. We are grateful to an anonymous reviewer, to Alexey Portnov and to the editor Daniel Praeg for the useful comments that helped strengthening the results of this study. We also thank Schlumberger for providing the Petrel software that was used for seismic display, interpretation and depth conversion. The open source QGIS software was used for bathymetric map and seismic profiles plotting, and MATLAB was used to calculate and plot the BGHSZ. The seafloor temperature data used in this study are from NOAA database and are available at https://www.nodc.noaa.gov/OC5/woa18f/. This project has been supported by the ACCORD funding scheme provided by the Natural Environment Research Council (NERC) as part of a National Capability, Official Development Assistance award (NC-ODA), NE/R000123/1.

Appendix A. Supplementary data

Supplementary data to this article can be found online at https://doi.org/10.1016/j.marpetgeo.2022.105690.

References

Akbar, M.A., 2011. An Assessment of the Geothermal Potential of Bangladesh. Geothermal Training Programme, Orkustofnun, Grensasvegur 9, Is-108 Reykjavik, Iceland, Reports, 5.

Alam, M., Alam, M.M., Curray, J.R., Chowdhury, M.L.R., Gani, M.R., 2003. An overview of the sedimentary geology of the Bengal Basin in relation to the regional tectonic framework and basin-fill history. Sediment. Geol. 155 (3–4), 179–208.

Andreassen, K., Hart, P.E., MacKay, M., 1997. Amplitude versus offset modeling of the bottom simulating reflection associated with submarine gas hydrates. Mar. Geol. 137, 25e40. https://doi.org/10.1016/S0025-3227(96)00076-X.

Arora, A., Cameotra, S.S., Balomajumder, C., 2015. Natural gas hydrate as an upcoming resource of energy. J. Petrol Environ. Biotechnol. 6 (1), 1–6. https://doi.org/10.4172/2157-7463.1000199.

Bastia, R., Das, S., Radhakrishna, M., 2010. Pre-and post-collisional depositional history in the upper and middle Bengal fan and evaluation of deepwater reservoir potential along the northeast Continental Margin of India. Mar. Petrol. Geol. 27 (9), 2051–2061. https://doi.org/10.1016/j.marpetgeo.2010.04.007.

Bear, J., 2013. Dynamics of Fluids in Porous Media. Courier Corporation ([book]).

Bengal Oil Development Co., LTD, 1978. BODC-3 Completion Report. Internal Report, pp. 1–39.

Berner, U., Poggenburg, J., Faber, E., Quadfasel, D., Frische, A., 2003. Methane in ocean waters of the Bay of Bengal: its sources and exchange with the atmosphere. Deep Sea Res. Part II Top. Stud. Oceanogr. 50 (5), 925–950.

Biot, M.A., 1956a. Theory of propagation of elastic waves in a fluid-saturated porous solid. I. Low-frequency range. J. Acoust. Soc. Am. 28, 168–178 https ://doi.org/10.1121/1.19082 39.

Biot, M.A., 1956b. Theory of propagation of elastic waves in a fluid-saturated porous solid. II. Higher frequency range. J. Acoust. Soc. Am. 28, 179–191 https ://doi.org/10.1121/1.19082 41.

Boswell, R., Collett, T., 2006. The gas hydrates resource pyramid. Nat. Gas Oil 304, 285–4541.

Boswell, R., Collett, T.S., 2011. Current perspectives on gas hydrate resources. Energy Environ. Sci. 4 (4), 1206–1215. https://doi.org/10.1039/C0EE00203H.

Boswell, R., Hancock, S., Yamamoto, K., Collett, T., Pratap, M., Lee, S.R., 2020. Natural gas hydrates: status of potential as an energy resource. In: Future Energy. Elsevier, pp. 111–131. https://doi.org/10.1016/B978-0-08-102886-5.00006-2.

Bourry, C., Chazallon, B., Charlou, J.L., Donval, J.P., Ruffine, L., Henry, P., Geli, L., Çagatay, M.N., Inan, S., Moreau, M., 2009. Free gas and gas hydrates from the Sea of Marmara, Turkey: chemical and structural characterization. Chem. Geol. 264 (1–4), 197–206. https://doi.org/10.1016/j.chemgeo.2009.03.007.

Brown, K.M., Bangs, N.L., Froelich, P.N., Kvenvolden, K.A., 1996. The nature, distribution, and origin of gas hydrate in the Chile Triple Junction region. Earth Planet Sci. Lett. 139 (3–4), 471–483. https://doi.org/10.1016/0012-821X(95)00243-6.

Brune, J.N., Curray, J., Dorman, L., Raitt, R., 1992. A proposed super-thick sedimentary basin, Bay of Bengal. Geophys. Res. Lett. 19 (6), 565–568. https://doi.org/10.1029/91GL03134.

Cartwright, J., Santamarina, C., 2015. Seismic characteristics of fluid escape pipes in sedimentary basins: implications for pipe genesis. Mar. Petrol. Geol. 65, 126–140. https://doi.org/10.1016/j.marpetgeo.2015.03.023.
Chabert, A., Minshull, T.A., Westbrook, G.K., Berndt, C., Thatcher, K.E., Sarkar, S., 2011. Characterization of a stratigraphically constrained gas hydrate system along the western continental margin of Svalbard from ocean bottom seismometer data. J. Geophys. Res. Solid Earth 116 (B12). https://doi.org/10.1029/2011JB008211.
Chand, S., Minshull, T.A., Gei, D., Carcione, J.M., 2004. Elastic velocity models for gas-hydrate-bearing sediments—a comparison. Geophys. J. Int. 159 (2), 573–590.
Chen, Q., Sidney, S., 1997. Seismic attribute technology for reservoir forecasting and monitoring. Lead. Edge 16 (5), 445–448. https://doi.org/10.1190/1.1437657.
Clennell, M.B., Hovland, M., Booth, J.S., Henry, P., Winters, W.J., 1999. Formation of natural gas hydrates in marine sediments: 1. Conceptual model of gas hydrate growth conditioned by host sediment properties. J. Geophys. Res. Solid Earth 104 (B10), 22985–23003. https://doi.org/10.1029/1999JB900175.
Coffin, M., Lawver, L., 1998. Atlas of Paleogeographic Reconstructions: the Plates Project Progress Report 215-0798. University of Texas at Austin, p. 75.
Collett, T.S., Boswell, R., Cochran, J.R., Kumar, P., Lall, M., Mazumdar, A., Ramana, M. V., Ramprasad, T., Riedel, M., Sain, K., Sathe, A.V., Vishwanath, K., 2014. Geologic implications of gas hydrates in the offshore of India: results of the national gas hydrate program expedition 01. Mar. Petrol. Geol. 58, 3–28. https://doi.org/10.1016/j.marpetgeo.2014.07.021.
Collett, T.S., Boswell, R., Waite, W.F., Kumar, P., Roy, S.K., Chopra, K., Singh, S.K., et al., 2019. India National Gas Hydrate Program Expedition 02 summary of scientific results: gas hydrate systems along the eastern continental margin of India. Mar. Petrol. Geol. 108, 39–142. https://doi.org/10.1016/j.marpetgeo.2019.05.023.
Collett, T.S., Johnson, A., Knapp, C., Boswell, R., 2009. Natural gas hydrates – a reviews. In: Collett, T., Johnson, A., Knapp, C., Boswell, R. (Eds.), Natural Gas Hydrates – Energy Resource Potential and Associated Geologic Hazards, vol. 89. American Association of Petroleum Geologists Memoir, p. 68.
Collett, T., Riedel, M., Cochran, J.R., Boswell, R., Kumar, P., Sathe, A.V., 2008. Indian Continental Margin Gas Hydrate Prospects: Results of the Indian National Gas Hydrate Program (NGHP) Expedition 01. https://doi.org/10.7916/d8-nf9w-cz91.
Cook, A.E., Sawyer, D.E., 2015. The mud-sand crossover on marine seismic data. Geophysics 80 (6), A109–A114. https://doi.org/10.1190/geo2015-0291.1.
Curiale, J.A., Covington, G.H., Shamsuddin, A.H.M., Morelos, J.A., Shamsuddin, A.K.M., 2002. Origin of petroleum in Bangladesh. AAPG Bull. 86 (4), 625–652. https://doi.org/10.1306/61EEDB66-173E-11D7-8645000102C1865D.
Curray, J.R., 1994. Sediment volume and mass beneath the Bay of Bengal. Earth Planet Sci. Lett. 125 (1–4), 371–383. https://doi.org/10.1016/0012-821X(94)90227-5.
Curray, J.R., 2014. The Bengal depositional system: from rift to orogeny. Mar. Geol. 352, 59–69. https://doi.org/10.1016/j.margeo.2014.02.001.
Curray, J.R., Emmel, F.J., Moore, D.G., 2003. The Bengal Fan: morphology, geometry, stratigraphy, history and processes. Mar. Petrol. Geol. 19 (10), 1191–1223. https://doi.org/10.1016/S0264-8172(03)00035-7.
Curray, J.R., Emmel, F.J., Moore, D.G., Raitt, R.W., 1982. Structure, tectonics, and geological history of the northeastern Indian Ocean. In: The Ocean Basins and Margins. Springer, Boston, MA, pp. 399–450.
Curray, J.R., Moore, D.G., 1971. Growth of the Bengal deep-sea fan and denudation in the Himalayas. Geol. Soc. Am. Bull. 82 (3), 563–572. https://doi.org/10.1130/0016-7606(1971)82[563:GOTBDF]2.0.CO;2.
Curray, J.R., Munasinghe, T., 1989. Timing of intraplate deformation, northeastern Indian Ocean. Earth Planet Sci. Lett. 94 (1–2), 71–77. https://doi.org/10.1016/0012-821X(89)90084-8.
De La Fuente, M., Vaunat, J., Marín-Moreno, H., 2020. A densification mechanism to model the mechanical effect of methane hydrates in sandy sediments. Int. J. Numer. Anal. Methods GeoMech. 44 (6), 782–802. https://doi.org/10.1002/nag.3038.
Deptuck, M.E., Sylvester, Z., 2018. Submarine fans and their channels, levees, and lobes. In: Submarine Geomorphology. Springer, Cham, pp. 273–299.
Dewangan, P., Sriram, G., Ramprasad, T., Ramana, M.V., Jaiswal, P., 2011. Fault system and thermal regime in the vicinity of site NGHP-01-10, Krishna–Godavari basin, Bay of Bengal. Mar. Petrol. Geol. 28 (10), 1899–1914. https://doi.org/10.1016/j.marpetgeo.2011.03.009.
Dickens, G.R., Quinby-Hunt, M.S., 1997. Methane hydrate stability in pore water: a simple theoretical approach for geophysical applications. J. Geophys. Res. Solid Earth 102 (B1), 773–783. https://doi.org/10.1029/96JB02941.
Duan, Z., Li, D., Chen, Y., Sun, R., 2011. The influence of temperature, pressure, salinity and capillary force on the formation of methane hydrate. Geosci. Front. 2 (2), 125–135. https://doi.org/10.1016/j.gsf.2011.03.009.
Dumke, I., Burwicz, E.B., Berndt, C., Klaeschen, D., Feseker, T., Geissler, W.H., Sarkar, S., 2016. Gas hydrate distribution and hydrocarbon maturation north of the Knipovich Ridge, western Svalbard margin. J. Geophys. Res. Solid Earth 121 (3), 1405–1424. https://doi.org/10.1002/2015JB012083.
Dvorkin, J., Nur, A., 1996. Elasticity of high-porosity sandstones; theory for two North Sea data sets. Geophysics 61, 1363–1370. https://doi.org/10.1190/1.14440 59.
Ecker, C., Dvorkin, J., Nur, A., 1998. Sediments with gas hydrates: internal structure from seismic AVO. Geophysics 63, 1659–1669 http s ://doi.org/10.1190/1.1444462.
Fauria, K.E., Rempel, A.W., 2011. Gas invasion into water-saturated, unconsolidated porous media: implications for gas hydrate reservoirs. Earth Planet Sci. Lett. 312 (1–2), 188–193. https://doi.org/10.1016/j.epsl.2011.09.042.
Fichler, C., Henriksen, S., Rueslaatten, H., Hovland, M., 2005. North Sea Quaternary morphology from seismic and magnetic data: indications for gas hydrates during glaciation? Petrol. Geosci. 11 (4), 331–337. https://doi.org/10.1144/1354-079304-635.
Foschi, M., Paganoni, M., Cartwright, J.A., Idiz, E., 2019. Microbial vs thermogenic gas hydrates in the South Falkland Basin: BSR distribution and fluid origin. Mar. Petrol. Geol. 102, 695–703. https://doi.org/10.1016/j.marpetgeo.2019.01.023.
GEBCO Compilation Group, 2019. GEBCO 2019 Grid. https://doi.org/10.5285/836f016a-33be-6ddc-e053-6c86abc0788e. https://www.gebco.net/. accessed on the 14th October 2019.
Ginsburg, G., Soloviev, V., Matveeva, T., Andreeva, I., 2000. 24. Sediment grain-size control on gas hydrate presence, sites 994, 995, and 9971. In: Proceedings of the Ocean Drilling Program, Scientific Results, pp. 237–245.
Grauls, D., 2001. Gas hydrates: importance and applications in petroleum exploration. Mar. Petrol. Geol. 18 (4), 519–523. https://doi.org/10.1016/S0264-8172(00)00075-1.
Guha, D.K., Henkel, H., Imam, B., 2010. Geothermal potential in Bangladesh-results from investigations of abandoned deep wells. April). In: Proceedings of the World Geothermal Congress, pp. 25–30. Bali, Indonesia.
Gullapalli, S., Dewangan, P., Kumar, A., Dakara, G., Mishra, C.K., 2019. Seismic evidence of free gas migration through the gas hydrate stability zone (GHSZ) and active methane seep in Krishna-Godavari offshore basin. Mar. Petrol. Geol. 110, 695–705. https://doi.org/10.1016/j.marpetgeo.2019.07.052.
Han, W.C., Chen, L., Liu, C.S., Berndt, C., Chi, W.C., 2019. Seismic analysis of the gas hydrate system at Pointer Ridge offshore SW Taiwan. Mar. Petrol. Geol. 105, 158–167. https://doi.org/10.1016/j.marpetgeo.2019.04.028.
Helgerud, M.B., Dvorkin, J., Nur, A., Sakai, A., Collett, T., 1999. Elastic-wave velocity in marine sediments with gas hydrates: effective medium modeling. Geophys. Res. Lett. 26 (13), 2021–2024. https://doi.org/10.1029/1999GL900421.
Henry, P., Thomas, M., Clennell, M.B., 1999. Formation of natural gas hydrates in marine sediments: 2. Thermodynamic calculations of stability conditions in porous sediments. J. Geophys. Res. Solid Earth 104 (B10), 23005–23022. https://doi.org/10.1029/1999JB900167.
Hillman, J.I., Cook, A.E., Daigle, H., Nole, M., Malinverno, A., Meazell, K., Flemings, P. B., 2017. Gas hydrate reservoirs and gas migration mechanisms in the Terrebonne Basin, Gulf of Mexico. Mar. Petrol. Geol. 86, 1357–1373. https://doi.org/10.1016/j.marpetgeo.2017.07.029.
Hiscott, R.N., Pickering, K.T., Bouma, A.H., Hand, B.M., Kneller, B.C., Postma, G., Soh, W., 1997. Basin-floor fans in the North Sea: sequence stratigraphic models vs. sedimentary facies: discussion. AAPG Bull. 81 (4), 662–665. https://doi.org/10.1306/522B4401-1727-11D7-8645000102C1865D.
Holbrook, W.S., Hoskins, H., Wood, W.T., Stephen, R.A., Lizarralde, D., 1996. Methane hydrate and free gas on the Blake Ridge from vertical seismic profiling. Science 273 (5283), 1840–1843. https://doi.org/10.1126/science.273.5283.1840.
Holland, M.E., Schultheiss, P.J., Roberts, J.A., 2019. Gas hydrate saturation and morphology from analysis of pressure cores acquired in the Bay of Bengal during expedition NGHP-02, offshore India. Mar. Petrol. Geol. 108, 407–423. https://doi.org/10.1016/j.marpetgeo.2018.07.018.
Hornbach, M.J., Saffer, D.M., Holbrook, W.S., 2004. Critically pressured free-gas reservoirs below gas-hydrate provinces. Nature 427 (6970), 142–144. https://doi.org/10.1038/nature02172.
Hovland, M., Gallagher, J.W., Clennell, M.B., Lekvam, K., 1997. Gas hydrate and free gas volumes in marine sediments: example from the Niger Delta front. Mar. Petrol. Geol. 14 (3), 245–255.
Hübscher, C., Spieß, V., 2005. Forced regression systems tracts on the Bengal Shelf. Mar. Geol. 219 (4), 207–218. https://doi.org/10.1016/j.margeo.2005.06.037.
Hutchison, I., 1985. The effects of sedimentation and compaction on oceanic heat flow. Geophys. J. Int. 82 (3), 439–459. https://doi.org/10.1111/j.1365-246X.1985.tb05145.x.
Hyndman, R.D., Davis, E.E., 1992. A mechanism for the formation of methane hydrate and seafloor bottom-simulating reflectors by vertical fluid expulsion. J. Geophys. Res. Solid Earth 97 (B5), 7025–7041. https://doi.org/10.1029/91JB03061.
Hyndman, R.D., Spence, G.D., 1992. A seismic study of methane hydrate marine bottom simulating reflectors. J. Geophys. Res. Solid Earth 97 (B5), 6683–6698.
Hustoft, S., Mienert, J., Bünz, S., Nouzé, H., 2007. High-resolution 3D-seismic data indicate focussed fluid migration pathways above polygonal fault systems of the mid-Norwegian margin. Mar. Geol. 245 (1–4), 89–106. https://doi.org/10.1016/j.margeo.2007.07.004.
Imam, M.B., Hussain, M., 2002. A review of hydrocarbon habitats in Bangladesh. J. Petrol. Geol. 25 (1), 31–52. https://doi.org/10.1111/j.1747-5457.2002.tb00098.x.
Ismail, M., Shamsuddin, A.H.M., 1991. Organic matter maturity and its relation to time, temperature and depth in the Bengal Foredeep, Bangladesh. J. Southeast Asian Earth Sci. 5, 381–390. https://doi.org/10.1016/0743-9547(91)90052-Y.
Judd, A.G., Hovland, M., 1992. The evidence of shallow gas in marine sediments. Continent. Shelf Res. 12 (10), 1081–1095.
Ketzer, M., Praeg, D., Rodrigues, L.F., Augustin, A., Pivel, M.A., Rahmati-Abkenar, M., Miller, D.J., Viana, A.R., Cupertino, J.A., 2020. Gas hydrate dissociation linked to contemporary ocean warming in the southern hemisphere. Nat. Commun. 11 (1), 1–9. https://doi.org/10.1038/s41467-020-17289-z.
Klauda, J.B., Sandler, S.I., 2005. Global distribution of methane hydrate in ocean sediment. Energy Fuel. 19 (2), 459–470.
Kroeger, K.F., Plaza-Faverola, A., Barnes, P.M., Pecher, I.A., 2015. Thermal evolution of the New Zealand Hikurangi subduction margin: impact on natural gas generation and methane hydrate formation–A model study. Mar. Petrol. Geol. 63, 97–114. https://doi.org/10.1016/j.marpetgeo.2015.01.020.
Kvenvolden, K.A., 1993. Gas hydrates—geological perspective and global change. Rev. Geophys. 31 (2), 173–187.

Kvenvolden, K.A., Barnard, L.A., 1983. Hydrates of natural gas in continental margins. In: Watkins, J.R., Drake, C.L. (Eds.), Studies of Continental Margin Geology, vol. 34. AAPG Mem, pp. 631–640.
Kvenvolden, K.A., Lorenson, T.D., 2001. The global occurrence of natural gas hydrates. In: Paull, C. (Ed.), Natural Gas Hydrates: Occurrence, Distribution, and Detection. Geophysical Monograph, vol. 124. American Geophysical Union, pp. 3–18. https://doi.org/10.1029/GM124p0003.
Lee, M.W., 2004. Elastic velocities of partially gas-saturated unconsolidated sediments. Mar. Petrol. Geol. 21 (6), 641–650. https://doi.org/10.1016/j.marpetgeo.2003.12.004.
Lindsay, J.F., Holliday, D.W., Hulbert, A.G., 1991. Sequence stratigraphy and the evolution of the Ganges-Brahmaputra delta complex. AAPG Bull. 75 (7), 1233–1254. https://doi.org/10.1306/0C9B291B-1710-11D7-8645000102C1865D.
Liner, C.L., McGilvery, T. A. (Mac), 2019. The Art and Science of Seismic Interpretation. Springer. https://doi.org/10.1007/978-3-030-03998-1.
Liu, X., Flemings, P.B., 2007. Dynamic multiphase flow model of hydrate formation in marine sediments. J. Geophys. Res. Solid Earth 112 (B3). https://doi.org/10.1029/2005JB004227.
Locarnini, R.A., Mishonov, A.V., Baranova, O.K., Boyer, T.P., Zweng, M.M., Garcia, H.E., Reagan, J.R., Seidov, D., Weathers, K.W., Paver, C.R., Smolyar, I.V., 2019. World ocean Atlas 2018. In: Mishonov, A., Technical (Eds.), NOAA Atlas NESDIS, vol. 1, p. 52pp, 81. https://www.nodc.noaa.gov/OC5/woa18f/.
Lopez, M., 2001. Architecture and depositional pattern of the Quaternary deep-sea fan of the Amazon. Mar. Petrol. Geol. 18 (4), 479–486. https://doi.org/10.1016/S0264-8172(00)00071-4.
Lorenson, T.D., Collett, T.S., 2018. National Gas Hydrate Program Expedition 01 offshore India; gas hydrate systems as revealed by hydrocarbon gas geochemistry. Mar. Petrol. Geol. 92, 477–492. https://doi.org/10.1016/j.marpetgeo.2017.11.011.
Lu, H., Seo, Y.T., Lee, J.W., Moudrakovski, I., Ripmeester, J.A., Chapman, N.R., Coffin, R. B., Gardner, G., Pohlman, J., 2007. Complex gas hydrate from the Cascadia margin. Nature 445 (7125), 303–306. https://doi.org/10.1038/nature05463.
Ma, H.X., Fan, G.Z., Shao, D.L., Ding, L.B., Sun, H., Zhang, Y., Zhang, Y.G., Cronin, B.T., 2020. Deep-water depositional architecture and sedimentary evolution in the Rakhine Basin, northeast Bay of Bengal. Petrol. Sci. 1–17 https://doi.org/10.1007/s12182-020-00442-0.
MacKay, M.E., Jarrard, R.D., Westbrook, G.K., Hyndman, R.D., 1994. Origin of bottom-simulating reflectors: geophysical evidence from the Cascadia accretionary prism. Geology 22 (5), 459–462. https://doi.org/10.1130/0091-7613(1994)022<0459:OOBSRG>2.3.CO;2.
MacLeod, M.K., 1982. Gas hydrates in ocean bottom sediments. AAPG (Am. Assoc. Pet. Geol.) Bull. 66 (12), 2649–2662. https://doi.org/10.1306/03B5AC8C-16D1-11D7-8645000102C1865D.
Mandal, R., Dewangan, P., Ramprasad, T., Kumar, B.J.P., Vishwanath, K., 2014. Effect of thermal non-equilibrium, seafloor topography and fluid advection on BSR-derived geothermal gradient. Mar. Petrol. Geol. 58, 368–381. https://doi.org/10.1016/j.marpetgeo.2014.04.002.
Marfurt, K.J., Sudhaker, V., Gersztenkorn, A., Crawford, K.D., Nissen, S.E., 1999. Coherency calculations in the presence of structural dip. Geophysics 64 (1), 104–111. https://doi.org/10.1190/1.1444508.
Marín-Moreno, H., Giustiniani, M., Tinivella, U., Piñero, E., 2016. The challenges of quantifying the carbon stored in Arctic marine gas hydrate. Mar. Petrol. Geol. 71, 76–82. https://doi.org/10.1016/j.marpetgeo.2015.11.014.
Marín-Moreno, H., Sahoo, S.K., Best, A.I., 2017. Theoretical modeling insights into elastic wave attenuation mechanisms in marine sediments with pore-filling methane hydrate. J. Geophys. Res. Solid Earth 122 (3), 1835–1847. https://doi.org/10.1002/2016JB013577.
Masud, M.H., Nuruzzaman, M., Ahamed, R., Ananno, A.A., Tomal, A.A., 2020. Renewable energy in Bangladesh: current situation and future prospect. Int. J. Sustain. Energy 39 (2), 132–175. https://doi.org/10.1080/14786451.2019.1659270.
Mavko, G., Mukerji, T., Dvorkin, J., 2009. Rock Physics Handbook—Tools for Seismic Analysis in Porous Media. Cambridge University Press.
Max, M.D., Johnson, A.H., 2014. Hydrate petroleum system approach to natural gas hydrate exploration. Petrol. Geosci. 20 (2), 187–199. https://doi.org/10.1144/petgeo2012-049.
Miles, P.R., 1995. Potential distribution of methane hydrate beneath the European continental margins. Geophys. Res. Lett. 22 (23), 3179–3182. https://doi.org/10.1029/95GL03013.
Milkov, A.V., Sassen, R., 2001. Estimate of gas hydrate resource, northwestern Gulf of Mexico continental slope. Mar. Geol. 179 (1–2), 71–83. https://doi.org/10.1016/S0025-3227(01)00192-X.
Miller, J.J., Lee, M.W., von Huene, R., 1991. An analysis of a seismic reflection from the base of a gas hydrate zone, offshore Peru (1). AAPG (Am. Assoc. Pet. Geol.) Bull. 75 (5), 910–924.
Minshull, T.A., Marín-Moreno, H., Betlem, P., Bialas, J., Buenz, S., Burwicz, E., Cameselle, A.L., et al., 2020. Hydrate occurrence in Europe: a review of available evidence. Mar. Petrol. Geol. 111, 735–764. https://doi.org/10.1016/j.marpetgeo.2019.08.014.
Moridis, G.J., 2003. Numerical studies of gas production from methane hydrates. Soc. Petrol. Eng. J. 32 (8), 359–370. https://doi.org/10.2118/75691-MS.
Moridis, G., Collett, T., 2003. Strategies for Gas Production from Hydrate Accumulations under Various Geologic Conditions. PROCEEDINGS, TOUGH Symposium 2003. Lawrence Berkeley National Laboratory, Berkeley, California. May 12–14, 2003.
Nixon, M.F., Grozic, J.L., 2007. Submarine slope failure due to gas hydrate dissociation: a preliminary quantification. Can. Geotech. J. 44, 314–325. https://doi.org/10.1139/t06-121.
Piper, D.J.W., Pirmez, C., Manley, P.L., Long, D., Flood, R.D., Normark, W.R., Showers, W., 1997. Mass-transport deposits of the Amazon fan. In: PROCEEDINGS-OCEAN DRILLING PROGRAM SCIENTIFIC RESULTS. NATIONAL SCIENCE FOUNDATION, pp. 109–146.
Pirmez, C., Hiscou, R.N., Kronen, J.K., 1997. Sandy turbidite successions at the base of channel-levee systems of the Amazon Fan revealed by FMS logs and cores: unraveling the facies architecture of large submarine fans. In: PROCEEDINGS-OCEAN DRILLING PROGRAM SCIENTIFIC RESULTS. NATIONAL SCIENCE FOUNDATION, pp. 7–34.
Portnov, A., Cook, A.E., Vadakkepuliyambatta, S., 2021. Diverse gas composition controls the Moby-Dick gas hydrate system in the Gulf of Mexico. Geology 49 (12), 1446–1451. https://doi.org/10.1130/G49310.1.
Portnov, A., Vadakkepuliyambatta, S., Mienert, J., Hubbard, A., 2016. Ice-sheet-driven methane storage and release in the Arctic. Nat. Commun. 7 (1), 1–7. https://doi.org/10.1038/ncomms10314.
Posewang, J., Mienert, J., 1999. The enigma of double BSRs: indicators for changes in the hydrate stability field? Geo Mar. Lett. 19 (1–2), 157–163.
Ramana, M.V., Ramprasad, T., Desa, M., Sathe, A.V., Sethi, A.K., 2006. Gas hydrate-related proxies inferred from multidisciplinary investigations in the Indian offshore areas. Curr. Sci. 183–189.
Ramana, M.V., Ramprasad, T., Paropkari, A.L., Borole, D.V., Rao, B.R., Karisiddaiah, S. M., Desa, M., Kocherla, M., Joao, H.M., Lokabharati, P., Gonsalves, M.J., Pattan, J. N., Khadge, N.J., Prakash Babu, C., Sathe, A.V., Sethi, A.K., 2009. Multidisciplinary investigations exploring indicators of gas hydrate occurrence in the Krishna–Godavari Basin offshore, east coast of India. Geo Mar. Lett. 29 (1), 25–38. https://doi.org/10.1007/s00367-008-0121-7.
Riedel, M., Collett, T.S., 2017. Observed correlation between the depth to base and top of gas hydrate occurrence from review of global drilling data. J. Geochem. Geochem., Geophys., Geosyst. 18, 2543–2561. https://doi.org/10.1002/2017GC006805.
Riedel, M., Bahk, J.J., Kim, H.S., Yoo, D.G., Kim, W.S., Ryu, B.J., 2013a. Seismic facies analyses as aid in regional gas hydrate assessments. Part-I: classification analyses. Mar. Petrol. Geol. 47, 248–268. https://doi.org/10.1016/j.marpetgeo.2013.04.011.
Riedel, M., Bahk, J.J., Kim, H.S., Scholz, N.A., Yoo, D.G., Kim, W.S., Ryu, B.J., Lee, S.R., 2013b. Seismic facies analyses as aid in regional gas hydrate assessments. Part-II: prediction of reservoir properties, gas hydrate petroleum system analysis, and Monte Carlo simulation. Mar. Petrol. Geol. 47, 269–290. https://doi.org/10.1016/j.marpetgeo.2013.04.012.
Riedel, M., Collett, T.S., Shankar, U., 2011. Documenting channel features associated with gas hydrates in the Krishna–Godavari Basin, offshore India. Mar. Geol. 279 (1–4), 1–11. https://doi.org/10.1016/j.margeo.2010.10.008.
Riedel, M., Goldberg, D., Guerin, G., 2014. Compressional and shear-wave velocities from gas hydrate bearing sediments: examples from the India and Cascadia margins as well as Arctic permafrost regions. Mar. Petrol. Geol. 58, 292–320. https://doi.org/10.1016/j.marpetgeo.2014.07.028.
Ruppel, C.D., 2011. Methane hydrates and contemporary climate change. Nat. Educt. Knowl. 2 (12), 12.
Ruppel, C.D., 2015. Permafrost-associated gas hydrate: is it really approximately 1% of the global system? J. Chem. Eng. Data 60 (2), 429–436. https://doi.org/10.1021/je500770m.
Ruppel, C.D., Kessler, J.D., 2017. The interaction of climate change and methane hydrates. Rev. Geophys. 55 (1), 126–168. https://doi.org/10.1002/2016RG000534.
Sahoo, S.K., Marín-Moreno, H., North, L.J., Falcon-Suarez, I., Madhusudhan, B.N., Best, A.I., Minshull, T.A., 2018. Presence and consequences of coexisting methane gas with hydrate under two phase water-hydrate stability conditions. J. Geophys. Res. Solid Earth 123, 3377–3390. https://doi.org/10.1029/2018JB015598.
Sain, K., Rajesh, V., Satyavani, N., Subbarao, K.V., Subrahmanyam, C., 2011. Gas-hydrate stability thickness map along the Indian continental margin. Mar. Petrol. Geol. 28 (10), 1779–1786. https://doi.org/10.1016/j.marpetgeo.2011.03.008.
Shedd, W., Boswell, R., Frye, M., Godfriaux, P., Kramer, K., 2012. Occurrence and nature of "bottom simulating reflectors" in the northern Gulf of Mexico. Mar. Petrol. Geol. 34 (1), 31–40. https://doi.org/10.1016/j.marpetgeo.2011.08.005.
Schwenk, T., Spieß, V., Breitzke, M., Hübscher, C., 2005. The architecture and evolution of the Middle Bengal Fan in vicinity of the active channel–levee system imaged by high-resolution seismic data. Mar. Petrol. Geol. 22 (5), 637–656. https://doi.org/10.1016/j.marpetgeo.2005.01.007.
Shipley, T.H., Houston, M.H., Buffler, R.T., Shaub, F.J., McMillen, K.J., Laod, J.W., Worzel, J.L., 1979. Seismic evidence for widespread possible gas hydrate horizons on continental slopes and rises. AAPG Bull. 63 (12), 2204–2213. https://doi.org/10.1306/2F91890A-16CE-11D7-8645000102C1865D.
Shukla, K.M., Kumar, P., Yadav, U.S., 2019. Gas hydrate reservoir identification, delineation, and characterization in the Krishna-Godavari basin using subsurface geologic and geophysical data from the national gas hydrate program 02 expedition, offshore India. Mar. Petrol. Geol. 108, 185–205. https://doi.org/10.1016/j.marpetgeo.2018.10.019.
Singh, S.C., Minshull, T.A., Spence, G.D., 1993. Velocity structure of a gas hydrate reflector. Science 260 (5105), 204–207. https://doi.org/10.1126/science.260.5105.204.
Sloan, E.D., 1998. Physical/chemical properties of gas hydrates and application to world margin stability and climatic change. Geol. Soc., Lond., Spec. Publ. 137 (1), 31–50. https://doi.org/10.1144/GSL.SP.1998.137.01.03.
Sloan, E.D., 2003. Fundamental principles and applications of natural gas hydrates. Nature 426 (6964), 353–359. https://doi.org/10.1038/nature02135.
Sloan, E.D., Koh, C.A., 2008. Clathrate Hydrates of Natural Gases, third ed. CRC Press-Taylor & Francis Group, Boca Raton, Florida.
Sprague, A.R.G., Garfield, T.R., Goulding, F.J., Beaubouef, R.T., Sullivan, M.D., Rossen, C., et al., 2005. Integrated Slope Channel Depositional Models: the Key to

Successful Prediction of Reservoir Presence and Quality in Offshore West Africa. CIPM, cuarto E-Exitep, p. 1e13.

Stanbrook, D., Bentley, M., 2022. Practical turbidite interpretation: the role of relative confinement in understanding reservoir architectures. Mar. Petrol. Geol. 135, 105372. https://doi.org/10.1016/j.marpetgeo.2021.105372.

Stern, L.A., Lorenson, T.D., Pinkston, J.C., 2011. Gas hydrate characterization and grain-scale imaging of recovered cores from the mount Elbert gas hydrate stratigraphic test well, Alaska north slope. Mar. Petrol. Geol. 28 (2), 394–403. https://doi.org/10.1016/j.marpetgeo.2009.08.003.

Stoll, R.D., Bryan, G.M., 1970. Wave attenuation in saturated sediments. J. Acoust. Soc. Am. 47, 1440–1447. https://doi.org/10.1121/1.19120 54.

Taner, M.T., Koehler, F., Sheriff, R.E., 1979. Complex seismic trace analysis. Geophysics 44 (6), 1041–1063. https://doi.org/10.1190/1.1440994.

Torres, M.E., Trehu, A.M., Cespedes, N., Kastner, M., Wortmann, U.G., Kim, J.H., Long, P., Malinverno, A., Pohlman, J.W., Riedel, M., Collett, T., 2008. Methane hydrate formation in turbidite sediments of northern Cascadia, IODP Expedition 311. Earth Planet Sci. Lett. 271 (1–4), 170–180. https://doi.org/10.1016/j.epsl.2008.03.061.

Wang, J., Zhang, L., Ge, K., Zhao, J., Song, Y., 2020. Characterizing anisotropy changes in the permeability of hydrate sediment. Energy 205, 117997. https://doi.org/10.1016/j.energy.2020.117997.

Westbrook, G.K., Chand, S., Rossi, G., Long, C., Bünz, S., Camerlenghi, A., Zillmer, M., 2008. Estimation of gas hydrate concentration from multi-component seismic data at sites on the continental margins of NW Svalbard and the Storegga region of Norway. Mar. Petrol. Geol. 25 (8), 744–758.

Yang, S.Y., Kim, J.W., 2014. Pliocene basin-floor fan sedimentation in the Bay of Bengal (offshore northwest Myanmar). Mar. Petrol. Geol. 49, 45–58. https://doi.org/10.1016/j.marpetgeo.2013.09.007.

You, K., Flemings, P.B., Malinverno, A., Collett, T.S., Darnell, K., 2019. Mechanisms of methane hydrate formation in geological systems. Rev. Geophys. https://doi.org/10.1029/2018RG000638.

Zhan, L., Guo, B., Yu, Y., 2019. Architectural elements and stratigraphy of a deepwater fan: a case study of the Bengal Fan, Rakhine Basin, offshore Myanmar. Arabian J. Geosci. 12 (6), 212. https://doi.org/10.1007/s12517-019-4378-0.